POST-TRANSCRIPTIONAL CONTROL OF RIPK1 IN MACROPHAGE INFLAMMATION AND NECROPTOSIS

ZIER ZHOU

Thesis submitted to the University of Ottawa
In partial fulfillment of the requirements for the
Master's degree in Biochemistry

Department of Biochemistry, Microbiology, and Immunology
Faculty of Medicine
University of Ottawa

ABSTRACT

Receptor-interacting protein kinase 1 (RIPK1) is a major upstream mediator of inflammation and cell death. These processes are key to common inflammatory diseases such as atherosclerosis, where macrophages play an important role in their progression. Closely linked to the expression of downstream genes, long non-coding RNAs (lncRNAs) are critical to controlling cellular processes in health and disease. As post-transcriptional regulatory mechanisms for RIPK1 are largely unknown, this project seeks to study the stability of *Ripk1* mRNA and RIPK1 protein, along with *Ripk1* mRNA interactions with relevant lncRNAs under various conditions. Using transcription and translation inhibitors, we determined that both *Ripk1* mRNA and RIPK1 protein are relatively unstable with half-lives of approximately 3 h. Their turnover in macrophages is further influenced by the timing and duration of inflammation. We also implemented a novel RNA pull-down procedure to capture *Ripk1* mRNA and attached lncRNAs for next-generation sequencing. Through differential expression analysis, we discovered significant upregulation of known lncRNA AC125611 and novel lncRNA MSTRG.5894.1 in *Ripk1*-targeted samples subject to inflammation. MSTRG.7477.1 was upregulated during necroptosis, while MSTRG.5684.5 was upregulated during both inflammation and necroptosis. GapmeR-mediated knockdowns of AC125611 and MSTRG.5684.5 under inflammatory conditions resulted in decreased *Ripk1* mRNA expression and RIPK1 protein expression, respectively. Meanwhile, MSTRG.7477.1 knockdowns were connected to decreased RIPK1 at both the mRNA and protein levels. Our research ultimately advances the current understanding of RIPK1 regulation by focusing on *Ripk1* mRNA-lncRNA associations and turnover of its mRNA and protein in macrophages, paving the way for future investigations into their capacity to act as therapeutic targets.

ACKNOWLEDGMENTS

I would first like to thank Dr. Katey Rayner for being an amazing research supervisor and helping steer my project in the right direction. Every time I leave a meeting with Katey, I feel simultaneously more excited and at ease about the uncertainty that permeates molecular biology. Katey is a key reason why my experiences in graduate school have been so positive, and I will be permanently thankful for all the support and opportunities she has given me.

I feel equally fortunate to be part of an extremely supportive lab environment at the Heart Institute. Many of my experiments would not have been possible without help from Michele Geoffrion, one of the most cheerful people I know. I would also like to thank Leah Susser, Dr. Adil Rasheed, and Cameron Stotts for setting brilliant examples as trainees, never hesitating to share their experiences and approaches to research. I cannot imagine working with a better team.

I would also like to thank professors Dr. Tommy Alain, Dr. Michele Ardolino, and Dr. Carolina Ilkow for taking the time to discuss my data and assess my progress as a master's student. Their thoughtful questions have led me to view my research topic from multiple angles, and their feedback on my results has allowed for improved clarity.

Finally, I am so grateful to my parents and friends for their endless support, honesty, and understanding through the ups, downs, and roundabouts of graduate school. The past two years have been important and unforgettable, as I have been able to learn more about science and life, how to research the parts that overlap, and how to balance the parts that do not.

TABLE OF CONTENTS

ABBREVIATIONS

ActD	Actinomycin D
ANOVA	Analysis of variance
ASO	Antisense oligonucleotide
BASO	Biotinylated ASO
BMDM	Bone marrow-derived macrophage
bp	Base pair
cDNA	Complementary DNA
CHX	Cycloheximide
ddPCR	Droplet digital PCR
DE	Differential expression
DMEM	Dulbecco's modified eagle medium
FPKM	Fragments per kilobase of transcript per million mapped reads
LDH	Lactate dehydrogenase
LncRNA	Long non-coding RNA
LPS	Lipopolysaccharide
miRNA	MicroRNA
mRNA	Messenger RNA
ncRNA	Non-coding RNA
NF-κB	Nuclear factor kappa B
NT	No treatment
nt	Nucleotide
qPCR	Quantitative polymerase chain reaction
RBP	RNA binding protein
RIN	RNA integrity number
RIPK1/3	Receptor-interacting protein kinase 1/3
RNase H	Ribonuclease H
rRNA	Ribosomal RNA
RT	Room temperature
SD	Standard deviation
SEM	Standard error of the mean
siRNA	Small interfering RNA
TLR4	Toll-like receptor 4
TNF-α	Tumor necrosis factor alpha
TNFR1	Tumor necrosis factor receptor 1
3'/5' UTR	3'/5' Untranslated region
zVAD	Benzyloxycarbonyl-Val-Ala-Asp-fluoromethylketone

LIST OF FIGURES

Introduction

Results

LIST OF TABLES

Main

Supplementary

1.0 INTRODUCTION

1.1 Receptor-interacting protein kinase 1 (RIPK1)

As an important member of the serine-threonine kinase family, receptor-interacting protein kinase 1 (RIPK1) is a multifunctional protein that controls multiple pathways related to inflammation, cell survival, and death (1, 2). With a molecular weight of 76 kDa, the protein comprises three key domains: a C-terminal death domain, an intermediate domain, and an N-terminal kinase domain (3). RIPK1 is encoded by the *Ripk1* gene (4) and resides in the cytoplasm of cells in various tissues, including the brain and heart (5).

Most of our understanding of its regulatory roles originates from studies on tumour necrosis factor (TNF) signaling (6). As a core component of TNF-induced signaling complexes that mediate nuclear factor kappa B (NF-κB) activation, apoptosis, and necroptosis, RIPK1 can paradoxically act as a scaffold to promote survival and as a kinase to activate cell death (**Figure 1**) (1, 7). RIPK1 activity is modified by mechanisms including phosphorylation, ubiquitylation, and deubiquitylation, all of which can determine whether a cell undergoes an inflammatory response or programmed cell death (2, 8).

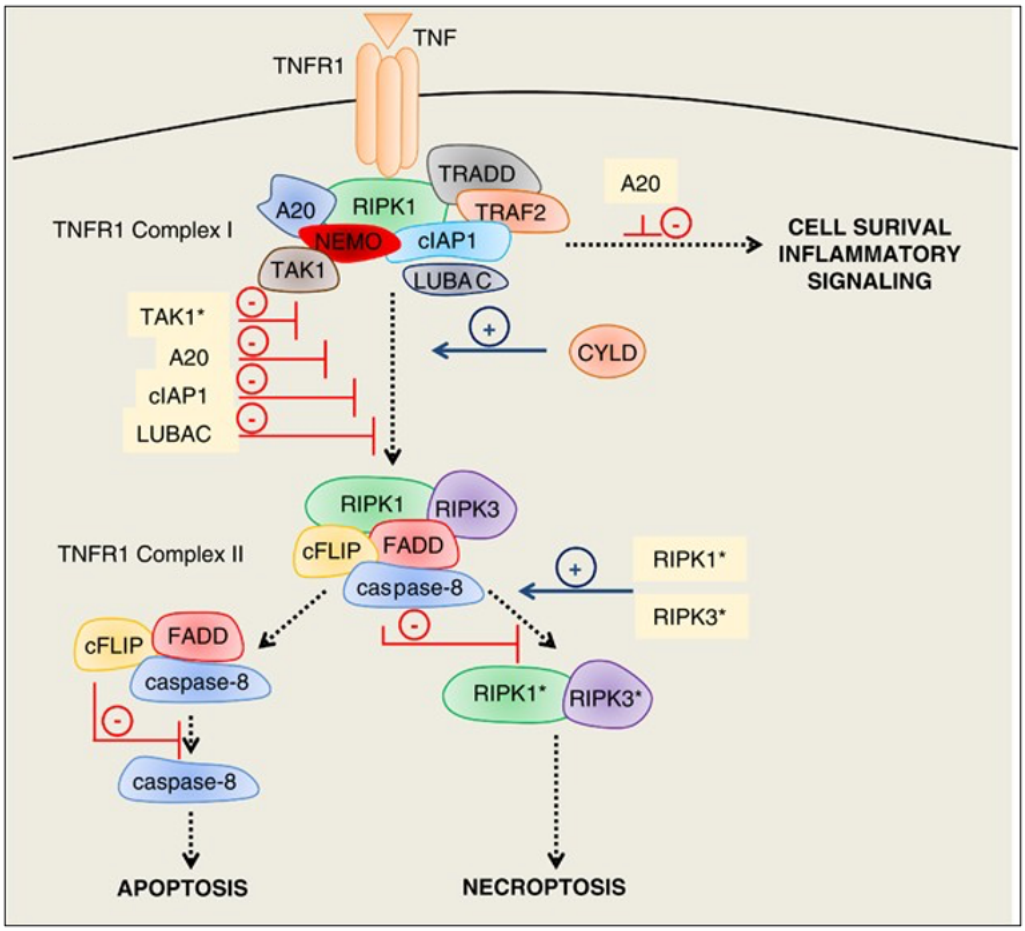

Figure 1. Signaling cascade for TNF-induced inflammation and cell death. When TNF binds TNFR1, complex I forms at the membrane to perform functions in cell survival and inflammatory signaling. The complex includes ubiquitin-editing enzyme A20, ubiquitylating enzyme cIAP1, linear ubiquitylating enzyme complex LUBAC, and TGF-β-activated kinase TAK1, all of which can negatively regulate cell death. Switching to the cytosolic death-inducing TNFR1 complex II involves the activity of deubiquitylating enzyme CYLD. Complex II composition determines whether the cell dies by apoptosis or necroptosis. Apoptotic machinery components FADD, c-FLIP, and caspase-8 suppress the activation of necroptosis, which in contrast requires the kinase activity of RIPK1 and RIPK3. Adapted from reference (9). CC BY-NC-ND 3.0.

1.1.1 RIPK1 scaffold in inflammation

Formation of complex I at the cytoplasmic membrane can either be initiated by TNF-α inducing TNF receptor 1 (TNFR1) or lipopolysaccharide (LPS) inducing toll-like receptor 4 (TLR4) (6). The latter interaction involves TRIF (toll/interleukin-1 receptor-domain-containing adaptor-inducing interferon-β), which in turn engages RIPK1 (10). Complex I is composed of RIPK1, TNFR1-associated death domain (TRADD), TNFR-associated factor 2 (TRAF2), and cellular inhibitor of apoptosis proteins 1/2 (cIAP1/2). When RIPK1 and TRADD bind TNFR1, TRADD recruits TRAF2 and cIAP1/2 to begin assembling the ubiquitin scaffold. Ubiquitylation is mainly carried out by cIAP1/2 and linear ubiquitin chain assembly complex (LUBAC), and deubiquitylation by cylindromatosis (CYLD) and A20 enzymes (11). Ubiquitin modifications located on various sites of RIPK1 can lead to dissimilar effects. Lys63- and Met1-linked polyubiquitin chains stabilize complex I for NF-κB signaling, whereas Lys48 ubiquitylation has been speculated to cause RIPK1 degradation (4, 12).

Complex I promotes cell survival when polyubiquitylated RIPK1 acts as a scaffold for kinase recruitment, including the IkB kinase (IKK) complex through IKKγ/NF-κB essential modulator (NEMO) (11). The formation of this trimeric complex, consisting of IKKα/β/γ, is mediated by IKKβ phosphorylation by transforming growth factor-β-activated kinase 1 (TAK1) (7). Phosphorylated IKKs then phosphorylate the inhibitory IkB protein bound to inactive NF-κB in the cytoplasm, triggering IkB degradation and NF-κB translocation to the nucleus and promoting pro-inflammatory gene transcription (7).

Ripk1$^{-/-}$ mice are known to die shortly after birth, likely due to the need for RIPK1 to perform scaffolding functions during development, and abnormal NF-κB signaling and cell death

patterns in its absence (13). More specifically, RIPK1 deficiency reduces NF-κB-mediated transcription of pro-survival proteins, including cIAP1, A20, and cellular FLICE-like inhibitory protein (cFLIP) (14). The kinase-independent scaffold structure of RIPK1 is also important for protecting cells from both apoptosis and necroptosis (7). This has been shown consistently using mice that express a catalytically inactive version of RIPK1, as they do not appear to develop any spontaneous overt phenotype and survive well into adulthood (7, 13).

In macrophages, RIPK1 plays a central role in regulating pro-inflammatory cytokine and chemokine production (15). However, excessive or prolonged inflammatory responses exacerbate tissue damage and disease progression (16). Furthermore, since many stimuli and receptors involved in pro-inflammatory cytokine expression likewise induce cell death, mixed responses between cells can occur (16). Whether they ultimately survive or die depends on a multitude of factors, including cell type, cellular contents, and regulatory mechanisms (17).

1.1.2 RIPK1 kinase in cell death

Cell death can take place alongside inflammation, as the immune system reacts to defend the host and repair their tissue (16). Apoptosis, the most popular form of programmed cell death, aims to counterbalance cell proliferation and eliminate unwanted cells without releasing harmful substances into their surroundings (18). Most cells in the human body die by apoptosis, which morphologically features plasma membrane blebbing, nuclear condensation and fragmentation, and apoptotic body budding (18). To maintain tissue homeostasis, these dead or dying cells express an “eat-me” signal on their surface to induce clearance by phagocytes (18).

RIPK1 is known to participate in the extrinsic pathway of apoptosis, which relies on activation ligands binding to death receptors and conformational changes consequently recruiting adaptors and caspases (19). This contrasts with the intrinsic pathway, which is triggered by intracellular injury or stress (19). When RIPK1 is deubiquitylated by CYLD, complex IIa is formed from interactions among Fas-associated protein with death domain (FADD), caspase-8, and RIPK1 (5). Derived from pro-caspase-8, active caspase-8 proceeds to activate downstream caspases to drive apoptosis and cleave RIPK1 to suppress necroptosis (5). This results in the destruction of cellular components in an immunologically silent manner, where compromised cells are efficiently removed (18).

Alternatively, necroptosis can eliminate dysfunctional cells when the default apoptotic mechanism is compromised (20). Triggers of necroptosis include death ligands and receptors that go on to activate specific molecular pathways. Fas ligand (FasL), TNF-α, and TNF-related apoptosis-inducing ligand (TRAIL) are known to interact with their respective receptors, Fas, TNFR1, and TRAILR (20). Although, the TNF-α/TNFR1 signaling cascade remains the most thoroughly studied pathway.

Following these early interactions under conditions of caspase-8 absence or inhibition, non-ubiquitylated RIPK1 and RIPK3 bind via their RIP homotypic interaction motif (RHIM) domains (7). This causes the phosphorylation of both RIPK1 and RIPK3, as well as necrosome or complex IIb formation with FADD (5). As an essential prerequisite to necrosome formation, RIPK1 kinase activation results in its autophosphorylation on multiple residues including Ser166, which has emerged as a biomarker for RIPK1 activation (21). Phosphorylated RIPK3 subsequently recruits and phosphorylates mixed lineage kinase domain-like (MLKL), which allows the

pseudokinase to create a pore-forming complex, as MLKL oligomers with a net positive charge bind negatively charged phospholipids of the plasma membrane (5, 22).

Necroptosis culminates in the loss of plasma membrane integrity, where damage-associated molecular patterns (DAMPs) exit the cell and proceed to activate innate immune cells (1). Typically released by dying cells, DAMPs can include proteins like high-mobility group box 1 (HMGB1), nucleic acids like mitochondrial DNA, and metabolites like ATP (1). These danger signals are then detected by pattern recognition receptors (PRRs), which induce cytokine and chemokine expression and further trigger a series of inflammatory signaling events (1, 16).

1.1.3 RIPK1 target in macrophages

RIPK1 is highly expressed in macrophages, which play central roles in tissue homeostasis and disease pathogenesis (21). These phagocytic cells of the immune system mediate the initial stages of inflammation and produce reactive oxygen species (ROS), which combat pathogens but also contribute to macrophage necroptosis (22). Because RIPK1 is known to upregulate in macrophages and mediate key processes, it has been targeted for many inflammatory and degenerative diseases (3, 5, 17).

In atherosclerosis, macrophages are the main cells that die throughout all stages of the disease (23). In its late stages, RIPK1-mediated necroptosis occurs and exacerbates plaque instability (24). Necrostatin-1 (Nec-1), a small-molecule inhibitor of RIPK1, has been used to impair necroptosis in atherosclerosis by blocking RIPK1 activity and preventing further inflammation (24). Alternatively, antisense oligonucleotides (ASOs) have been administered to knock down RIPK1 and protect against the progression of atherosclerosis (25).

As the first and main form of immune defense in the brain, microglia are macrophages that play a central role in neurodegenerative diseases such as Alzheimer's. RIPK1 upregulation has also been observed in these cells, and inhibition of its kinase activity by Nec-1 stable (Nec-1s) was found to reduce neuroinflammation and amyloid plaque formation (26). Overall, the findings above highlight RIPK1 in macrophages as a strong contributor to multiple chronic inflammatory diseases and a potentially important therapeutic target.

1.2 Post-transcriptional gene regulation

Gene expression is a complex process that is controlled at multiple levels, while post-transcriptional regulation occurs at any stage after the messenger RNA (mRNA) is transcribed (27, 28). Non-coding RNAs (ncRNAs), which do not code for proteins, are known to participate in these processes (28). Knowledge of long non-coding RNAs (lncRNAs) is limited, in part because their regulatory functions are typically broader and more complex than microRNAs (miRNAs), their more widely studied counterparts (29).

Post-transcriptional control also entails the turnover of gene products, including mRNA and protein (27, 28). mRNA turnover can directly affect translation and the amount of protein being produced, which is connected to protein turnover and activity within the cell (**Figure 2**) (30, 31). The balance between protein synthesis and degradation is tightly regulated as well, allowing the cell to conserve its limited energy and adapt quickly to changing conditions (32).

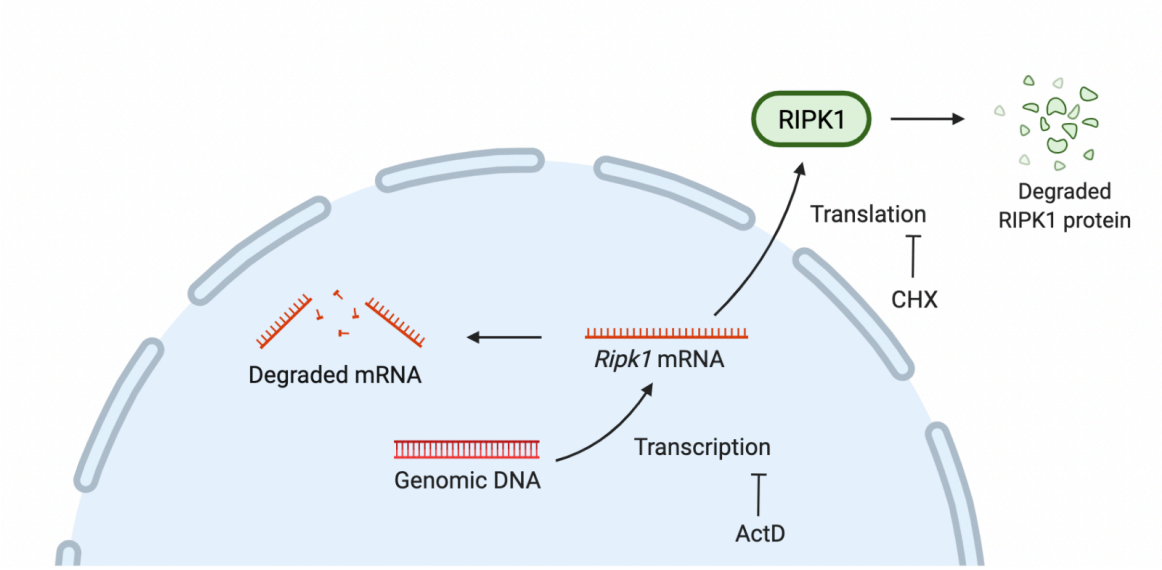

Figure 2. Transcription, translation, and turnover of *Ripk1* mRNA and RIPK1 protein in the cell. Transcription takes place in the nucleus and is mainly performed by RNA polymerase II. Once processed, *Ripk1* mRNA is transported into the cytoplasm and loaded onto ribosomes for translation into RIPK1 protein. Global transcription and translation can be inhibited by actinomycin D (ActD) and cycloheximide (CHX) to study mRNA and protein turnover, respectively.

1.2.1 mRNA turnover

mRNA turnover is a key component of gene expression control that alters transcript abundance and eventually protein function within a cell (28). Large-scale analyses reveal that up to 50% of gene expression changes in response to cellular signals occur at the level of mRNA stability (33). Balancing mRNA decay and synthesis is crucial for the correct functioning of various biological processes to maintain homeostasis (30, 34). Another reason for keeping certain mRNAs inherently unstable is to facilitate rapid changes in their abundance when necessary (34).

In general, mRNA decay in eukaryotic cells starts with deadenylation and/or decapping of the mature mRNA, followed by degradation by exonucleases (34). The first step in the mRNA turnover pathway involves shortening the 3' poly(A)tail and is uniquely reversible, as transcripts with the right signals can be re-adenylated and returned to polysomes (34). Following deadenylation, one of two irreversible routes is taken. Either the 5' cap is removed by de-capping, which enables mRNA decay in the 5'→3' direction by exoribonuclease 1 (XRN1), or the unprotected 3' end is attacked by a large complex of 3'→5' exonucleases, coined as the exosome (34).

Deadenylation, decapping, and degradation are modulated by regulatory factors that largely determine the stability of mRNA transcripts (30). Variables influencing their susceptibility to degradation machinery include mRNA-specific sequences and structural features, which can be recognized by nucleases and RBPs (30, 34). As one of the most common determinants of RNA stability, AU-rich elements (AREs) are short sequences of adenine and uridine bases that commonly reside in the 3' untranslated region (UTR) of mRNAs (30). AREs exhibit their

destabilizing functions by recruiting ARE-binding proteins, which drive the transcript to degradation (30, 34).

Eukaryotic mRNA turnover and translational control frequently take place in cytoplasmic sites called processing bodies (P bodies), where proteins related to deadenylation, decapping, and other degradation machinery localize (34, 35). These structures have also been found to sequester mRNAs for temporary storage, allowing them to later exit when needed for translation (34, 35). Although P bodies are important in mRNA-mediated gene silencing, they are not required for function but rather a consequence of controlling mRNA activity (36).

Regulation of mRNA half-life further involves ncRNAs, including lncRNAs, which may differ between cell types or signaling patterns within a certain cell (37). LncRNAs can determine the rate of mRNA decay, either directly by promoting or precluding decay factor binding, or indirectly by influencing the translational status of the mRNA (30). For example, 1/2-sbsRNAs (half-Staufen 1-binding site lncRNAs) recruit Staufen (STAU1), an RBP that recognizes the 3′ UTR of mRNAs, to mediate their degradation (38).

Interestingly, mRNA turnover has also been discovered to influence its targetability by small RNAs such as miRNAs and siRNAs (small interfering RNAs) (39). Notwithstanding the positive correlation between abundance and targetability, mRNAs with high turnover rates are harder to repress, regardless of their steady-state levels (39). Understanding how mRNA half-lives may impact mRNA expression levels according to lncRNA changes in the cell is useful for upcoming transfections as well as possible therapeutic interventions (39).

1.2.2 Protein turnover

In the face of varying stresses or stimuli, proteins within cells are continually being degraded and replaced by newly synthesized proteins to maintain homeostasis (32). This process is highly selective and precisely regulated, as individual proteins are destroyed at widely different rates (40). Half-lives can range from seconds to days but fall near several hours for most proteins (28, 41). Determining a given protein's turnover is one of the first steps toward understanding how its cellular abundance and activity are controlled under specific conditions (42).

Protein half-life also relates to the N-end rule, which defines the destabilizing activity of a particular amino-terminal residue and its post-translational modification (43). The pathway identifies proteins with degradation signals or degrons marked by ubiquitin, facilitating their breakdown by a multi-subunit complex known as the 26S proteasome (43). The N-end rule pathway has also been found to counteract cell death by destroying pro-apoptotic protein fragments. Using RIPK1 to illustrate, Cys-RIPK1 bears a destabilizing N-terminal residue that helps regulate its kinase activity and downstream reactions leading to apoptosis (44).

Compared to translational control, protein stability holds a minor role in determining protein abundance within a cell (31). Research shows that 40% of the variability in protein levels is attributed to the variability in mRNA levels (28). Considering the high energy costs associated with protein synthesis, it makes sense to prioritize and optimize regulatory mechanisms earlier on in the gene expression pathway (28).

Nevertheless, protein turnover features particular advantages such as speed and irreversibility (28, 45). Proteins with short half-lives require relatively less time to reach a new

steady-state level following a change in their synthesis rate (45). In certain scenarios, the ability to respond quickly may outweigh the more energetically frugal but slower activation of genes starting from transcription (28). Irreversible degradation also eliminates any chance of the protein being inappropriately reactivated (45).

Protein and mRNA stability often connect to their physiological functions, suggesting that their half-lives evolved under similar energetic and dynamic constraints (31). Housekeeping genes tend to have stable proteins and mRNAs, which can be explained by the energy demands associated with translation and transcription (31, 46). In contrast, regulatory genes regularly encode unstable mRNAs and proteins that are only required for a limited time in the cell (31, 46). Since mRNAs and proteins are information carriers, their degradation can be interpreted as built-in timers for controlling the persistence of genetic information (31). This is especially helpful for signaling molecules that are actively being used, or those that must adjust their expression rapidly in response to a stimulus (31).

1.2.3 Long non-coding RNAs

About 80% of transcribed ncRNAs are lncRNAs, which are defined as non-coding transcripts longer than 200 nucleotides (nt) that can regulate many physiological processes (29, 47). LncRNAs tend to display cell- or tissue-specific expression patterns and dysregulation under pathological conditions (48). Their functions usually depend on whether they localize in the nucleus or cytoplasm, as well as their structure or complementarity with other nucleic acids (49, 50). Nuclear lncRNAs frequently modulate transcriptional activities such as chromatin remodeling, whereas cytoplasmic lncRNAs mediate signal transduction pathways and translational programs (50).

In contrast to *cis*-acting lncRNAs that control the expression of nearby genes, *trans*-acting lncRNAs are understood to function away from their transcription sites (51). Many *trans*-acting lncRNAs are post-transcriptional regulators, playing roles in mRNA processes that include splicing, turnover, and translation (52). Some examples of mRNA-lncRNA interactions are illustrated in **Figure 3**. Briefly, LncRNAs can repress splicing by forming duplexes with target pre-mRNAs to block distinct binding sites that would otherwise be recognized by the spliceosome (53). LncRNAs can also promote mRNA degradation by partial base-pairing to recruit certain RNA-binding proteins (RBPs) (54), or even boost protein translation by loading other RBPs onto active polyribosomes (55). These RBPs may be methyltransferases (writers) and demethylases (erasers) involved in N^6-methyladenosine (m^6A) methylation (56). As the most prevalent mRNA modification in eukaryotes, m^6A is further recognized by RBPs (readers) to regulate mRNA metabolism and stability (37, 56).

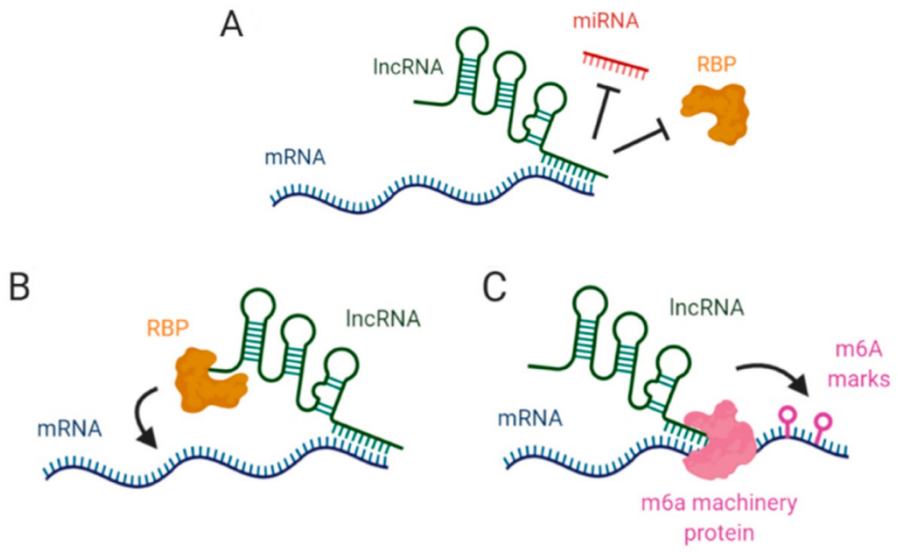

Figure 3. Mechanisms by which lncRNAs can regulate mRNA stability and gene expression. Main mechanisms of action include: (**A**) directly interacting with the target mRNA to block miRNA- or RBP-binding sites; (**B**) serving as a scaffold to enhance RBP-mRNA interactions; and (**C**) associating with m6A machinery to modulate m6A levels of target mRNAs. Adapted from reference (37). CC-BY 4.0.

Moreover, lncRNAs can act as competitive endogenous sponges for specific miRNAs, preventing them from disrupting the stability or translation of target mRNA transcripts (49). One of these lncRNAs is named necrosis-related factor (NRF) and blocks miR-873 from inhibiting RIPK1 and RIPK3 translation (57). Knocking down NRF in cardiomyocytes resulted in reduced RIPK1/RIPK3-mediated necroptosis during ischemia-reperfusion (I/R) injury (57). In addition, this strategy can work in reverse, where lncRNAs compete with miRNAs by masking sites on mRNA (37).

LncRNAs are encoded by a large proportion of the mammalian genome and can be classified according to their different genomic locations (58). Intergenic lncRNAs (lincRNAs) are transcribed from non-coding regions and do not overlap with protein-coding genes. Conversely, sense, antisense, and intronic lncRNAs overlap with coding regions and originate from the sense strand, antisense strand, and introns, respectively (58). Present studies focus most on lincRNAs and then antisense lncRNAs, while less is known about intronic and sense lncRNAs (58).

Like mRNAs, lncRNAs are normally transcribed by RNA polymerase II, capped by 7-methyl guanosine (m7G) at their 5' ends, and polyadenylated at their 3' ends (52). After being processed and modified, mature lncRNAs assume specific secondary and higher-order structures (59). Although these mRNA-like features contribute to the ability of many lncRNAs to exit the nucleus and enter pathways in which mRNAs take part (60), lncRNAs still tend to be less efficiently spliced and contain fewer exons than mRNAs (52).

Compared to canonical protein-coding genes, lncRNAs are lowly expressed and poorly conserved at the sequence level (58, 60). However, studies report that their secondary and tertiary structures are highly conserved and may be related to their biological functions (29, 59).

Furthermore, a lack of sequence conservation does not automatically imply no functionality because many lncRNA mechanisms of action have low sequence constraints (60). For instance, sequestering some RBPs only requires conservation over short sections of the total sequence, within the range of 10 nt (60). LncRNAs are also conserved in terms of regulatory function, which often correlates with their structure and subcellular localization (61). Furthermore, lncRNAs can show syntenic conservation when transcribed from gene loci in the same chromosomal location of different species (60).

The human genome is believed to contain over 16,000 lncRNA genes, but most of their functions remain unknown (52). Despite the growing catalog of lncRNAs, most transcribed products that have been detected have yet to be functionally annotated, partly due to the difficulty of capturing lncRNAs and distinguishing functional transcripts from transcriptional noise (62). Other challenges can be attributed to their relatively low abundance and poor conservation (62).

Despite these limitations, lncRNAs can be decisive in activating or blocking the expression of inflammatory genes that contribute to immune responses and cellular homeostasis (63). Compared to proteins, lncRNAs may be superior targets, as their fast turnover, high tissue specificity, and regulation of specific cellular networks likely lead to less toxic side effects (52). More rapid effects with lower doses are further feasible, given the lack of translation and low expression of lncRNAs (52). For these reasons, lncRNAs are regarded as promising for therapeutic targeting, and research is steadily progressing toward the development of clinical applications.

2.0 RATIONALE, HYPOTHESIS, AND OBJECTIVES

2.1 Rationale

RIPK1 is a multifunctional protein that regulates signaling pathways for inflammation, cell survival, and cell death. Usually correlated with its mRNA and protein expression, RIPK1 levels vary according to different stimuli and elevate in many inflammatory diseases with macrophages as key players in their progression. While post-translational modifications such as ubiquitylation and phosphorylation can determine downstream actions of RIPK1, how the molecule is controlled at the post-transcriptional level is unclear. Given this gap, it is of great interest to study RIPK1 in macrophages under normal and inflammatory conditions by analyzing its related lncRNAs, as well as mRNA and protein turnover rates.

2.2 Hypothesis

Both *Ripk1* mRNA and RIPK1 protein stability play important roles in post-transcriptionally regulating RIPK1 under normal and inflammatory conditions. Distinct lncRNAs interacting with *Ripk1* mRNA also regulate RIPK1 in macrophage inflammation and necroptosis.

2.3 Objectives

1. To understand how RIPK1 levels are regulated by the turnover of its mRNA and protein in macrophages under normal and inflammatory conditions
2. To design and optimize an experimental method for pulling down RNA to analyze *Ripk1* mRNA and attached lncRNAs in inflammation and necroptosis

3.0 MATERIALS AND METHODS

3.1 Cell culture

RAW 264.7 mouse macrophages were maintained in Dulbecco's modified eagle medium (DMEM) and stored inside a 37°C, 5% CO_2 incubator. 10% fetal bovine serum (FBS) and 1% penicillin/streptomycin (P/S) were added as supplements.

3.2 Cell treatments

Macrophages were plated at a density of 1×10^6 cells/ml in 6-well plates with 2 ml media in each well. Inflammatory and necroptotic conditions were induced using 100 ng/ml LPS in the presence or absence of 50 μM zVAD, an irreversible pan-caspase inhibitor that blocks apoptosis. Treatments were delivered for either 6 h or 10 h in DMEM supplemented with 1% FBS and 1% P/S to slow cell growth in the process.

3.3 Cytotoxicity assays

Cytotoxicity assays were determined by monitoring lactate dehydrogenase (LDH) release, as outlined in another study (24). Briefly, treated samples were collected and centrifuged at 12,000 xg for 5 min at room temperature (RT) to remove cell debris. Once LDH assay buffer (1x PBS, 0.02% NADH, 0.03% sodium pyruvate) was added to the media, LDH levels were measured using a kinetic assay. This was done by recording changes in absorbance at 340 nm for 10 min at 1-min intervals. The slope of the curve indicates the extent of cell death, which is expressed as fold change relative to the control.

3.4 mRNA decay assays

mRNA degradation experiments involved using actinomycin D (ActD), which binds DNA at the transcription initiation complex to prevent elongation by RNA polymerase (64). RAW 264.7 cells were either pre-treated with 100 ng/ml LPS for 10 h and then treated with 10 μg/ml ActD (A9415, Sigma-Aldrich), or treated with LPS at the same time ActD was first added. NT controls and LPS-treated cells were collected after 0, 1, 2, and 4 h of administering ActD for RNA extraction and quantitative polymerase chain reaction (qPCR) analysis. Data points were normalized to the t=0 h time point and presented as a percentage (%) of remaining *Ripk1* mRNA, leading to half-life calculations by linear regression.

3.5 Reverse transcription and qPCR

Complementary DNA (cDNA) was synthesized using iScript Reverse Transcription Kit (Bio-Rad) and isolated RNA ranging from 100 ng to 1 μg, based on the concentrations available. The Mastercycler Gradient (Eppendorf) program for cDNA synthesis involves: (i) primer annealing by incubating samples for 5 min at 25°C; (ii) reverse transcription for 30 min at 42°C; and (iii) enzyme inactivation for 10 min at 85°C. qPCR was then performed on the Mastercycler Realplex 2 (Eppendorf). Thermal cycling features 40 cycles of the following steps: (i) denaturation for 15 s at 95°C; (ii) annealing for 15 s at 60°C; and (iii) extension for 20 s at 70°C. SsoAdvanced Universal SYBR Green Supermix (Bio-Rad) was used to bind double-stranded DNA (dsDNA) and measure fluorescence for quantification. *Ripk1* gene expression was quantified using primers from Invitrogen (forward: 5’ GAAGACAGACCTAGACAGCGG 3’; reverse: 5’ CCAGTAGCTTCACCACTCGAC 3’) and normalized to signal recognition particle 14 (*Srp14*).

3.6 Cycloheximide chase assays

Like above, macrophages were first stimulated with 100 ng/ml LPS for 10 h or later co-stimulated simultaneously with cycloheximide (CHX), which binds ribosomes to block the elongation step of protein translation. 20 μg/ml CHX (2112S, Cell Signaling Technology) was added to unstimulated and LPS-stimulated cells at 0, 3, 6, and 9 h time points. All samples were then collected for protein analysis.

3.7 Protein preparation and western blotting

Cells were rinsed in cold 1x phosphate-buffered saline (PBS) and lysed in 100 μl of radioimmunoprecipitation assay (RIPA) buffer with freshly added protease inhibitors. Samples were centrifuged at 21,000 xg to clear lysates of cellular debris. Supernatants were collected and stored at −20 °C before quantifying with the Pierce 660-nm Protein Assay Kit. Protein aliquots were adjusted to equivalent amounts (12-20 μg) and volumes (25-35 μl) when combined with 5x loading buffer and heated at 95°C for 5 min. Samples were resolved on 10% sodium dodecyl sulfate-polyacrylamide gel electrophoresis (SDS-PAGE) gels and transferred to nitrocellulose membranes (Bio-Rad). Membranes were blocked at RT for 1 h with 5% (w/v) skim milk in 1x Tris-buffered saline with 0.1% Tween (TBS-T). This was followed by antibody incubations with 1% milk at 4 °C overnight for mouse anti-RIP (610459, BD Biosciences; 1:1,000 dilution). For loading control antibodies, membranes were incubated with either rabbit anti-β-actin (4970, Cell Signaling Technology; 1:10,000 dilution) or mouse anti-HSP 90α/β (sc-13119, Santa Cruz Biotechnology; 1:1,000 dilution) on a rocker platform at RT for 1 h. After each incubation, membranes were washed with TBS-T three times for 10 min. Anti-mouse or anti-rabbit horseradish peroxidase (HRP) conjugated secondary antibodies were later diluted 1:2,000 in 1%

milk and membranes were incubated again at RT for 1 h. TBS-T washes were repeated before finally adding Clarity Western ECL peroxide and luminol/enhancer reagents (Bio-Rad) to detect proteins via enhanced chemiluminescence (ECL). Image Lab software (Bio-Rad) was used to visualize bands and analyze intensity. Once normalized against β-actin or HSP 90α/β expression, RIPK1 protein bands were quantified as a % of starting levels under given conditions.

3.8 ASO probe and qPCR primer designs

The full *Ripk1* transcript sequence was obtained from the Ensembl genome browser and visualized on the RNAfold web server. ASOs (about 22 nt in length) were designed to bind multiple exon-exon junctions and the 3' UTR of *Ripk1* mRNA. To optimize these interactions, ASO-specific sections were selected for having low steric hindrance by neighbouring RNA secondary structures (65). Forward and reverse qPCR primers were subsequently designed to span these sections. Primers were selected and modified using SeqBuilder Pro software (v17.2.1) according to the standard guidelines. Ideal amplification is achieved when primers have a melting temperature near 60°C and a length between 18–25 base pairs (bp) for high specificity, and GC content between 40–60% for preferred stability (66). SeqBuilder also located potential secondary structure interactions to minimize the formation of dimers and hairpins that would otherwise interfere with the qPCR reaction. Custom sequences for ASOs (**Table S1**) and qPCR primers (**Table S2**) were ordered from Integrated DNA Technologies.

3.9 ASO binding validation assays

To test the ability of our ASOs to bind *Ripk1* mRNA, validation assays were performed with cell lysates incubated with or without ribonuclease H (RNase H) from Thermo Fisher

Scientific. After washing with cold 1x PBS, macrophages were scraped from their plates and transferred into 1.5 ml Eppendorf tubes to centrifuge at 500 xg for 3 min at 4°C. Another PBS wash was done before resuspending the pellet in lysis buffer (50 mM Tris-HCl, 150 mM NaCl, 0.5% NP-40, 1x Roche cOmplete Protease Inhibitor Cocktail). These samples were incubated for 30 min on ice and centrifuged at 21,000 xg for 5 min at 4°C. Supernatants were subsequently combined with 10x RNase H buffer, 5 M NaCl, and 1x RNase Inhibitor (Thermo Fisher Scientific) in RNase-free water to adjust the total sample volume to 1 ml. 100 pmol of each ASO was pipetted into separate samples, all of which were incubated on a tube rotator for 2 h at 4°C. After incorporating 2.5 U of RNase H into certain samples, they were placed inside an Innova 42 Incubator Shaker (Eppendorf) for 20 min at 350 rpm. 700 µl of TriPure Isolation Reagent (Roche) was then added to isolate RNA for further validation by qPCR. When successful binding occurs between an ASO and *Ripk1* mRNA, RNase H is expected to cleave the DNA-RNA duplex and cause RNA degradation, as evidenced by the lower qPCR detection compared to the control with no ASO.

3.10 Droplet digital PCR

With higher sensitivity compared to qPCR, droplet digital PCR (ddPCR) allowed for *Ripk1* quantification following RNA pull-downs. Reactions were prepared by combining cDNA templates with EvaGreen Supermix (Bio-Rad), RNase-free water, and custom-made *Ripk1* primers (forward: 5’ CTGATGCACGTGCTAAAGACCCAG 3’; reverse: 5’ GCCTCCACGATTATCCTTCCTTTC 3’). Samples along with Droplet Generation Oil (Bio-Rad) were loaded into specified wells of a DG-8 ddPCR cartridge (Bio-Rad) and emulsified in the QX200 Droplet Generator (Bio-Rad). Once each reaction was partitioned into approximately

20,000 droplets, samples were transferred to a 96-well plate and sealed with foil at 180°C using a PX1 PCR Plate Sealer (Bio-Rad). PCR amplification was performed on a C1000 Touch Thermal Cycler (Bio-Rad). Afterwards, samples entered the QX200 Droplet Reader (Bio-Rad), which measured fluorescence to determine the number of positive and negative droplets, depending on whether the target is present. The fraction of positive events was eventually fitted to a Poisson distribution on QuantaSoft software to calculate target concentrations (copies/µl).

3.11 RNA pull-down experiments

Macrophages at 90% confluency were either untreated or treated with previously indicated concentrations of LPS +/- zVAD for 10 h and washed with 1x PBS. Cells were collected from two 15-cm dishes and lysed in polysome extraction buffer (PEB; 20 mM Tris-HCl, 100 mM KCl, 5 mM $MgCl_2$, 0.5% NP-40). 1x protease inhibitor, 1x RNase inhibitor, and 2x TENT (20 mM Tris-HCl, 2 mM EDTA, 500 mM NaCl, 1% Triton X-100) were added to PEB on the day of the experiment. After placing samples on ice for 10 min and spinning at 10,000 rpm for 15 min at 4°C, supernatants were transferred into new 1.5 ml Eppendorf tubes and combined with 500 µl of 2x TENT buffer. For each treatment, one sample received 200 pmol of 3' biotinylated ASOs (BASOs) targeting *Ripk1* mRNA while the other received 200 pmol of a scrambled control BASO. The non-targeting control sequence 5' CCTTCCCTGAAGGTTCCTCC 3' was obtained from another study (25). All samples were then incubated for 2 h at RT with rotation. Using a magnetic stand, preparation of Dynabeads M-280 Streptavidin (Invitrogen) involved washing twice with 500 µl of Solution A (0.1 M NaOH, 0.05 M NaCl), once with Solution B (0.1 M NaCl), and finally once with 1x TENT buffer (2x TENT diluted 1:1 with PEB). Cleaned magnetic beads were mixed with treated lysates, incubated for 1 h, and then centrifuged at 5,500 rpm for 5 min at 25°C. After

removing the supernatant and washing three times with 1x TENT, the beads were spun down again to remove any remaining buffer and ready for RNA isolation.

3.12 RNA isolation

Total RNA was isolated by adding TriPure Isolation Reagent (Roche) to macrophages following media removal. Next, supernatants were collected in 1.5 ml Eppendorf tubes and combined with chloroform. After shaking this mixture and incubating for 10 min at RT, samples were spun at 12,000 xg for 15 min at 4°C. The clear upper layer containing RNA was transferred into another tube for washing with isopropanol and 70% ethanol. These steps were followed by centrifugation at 12,000 xg for 10 min and 7,500 xg for 5 min, respectively. Once the RNA pellet was visible and air-dried at RT for 10 min, it was resuspended in 20-50 µl of RNase-free water, with the volume depending on pellet size.

3.13 RNA assessments

RNA concentrations (ng/ml) were determined by pipetting 1 µl samples into the NanoDrop 1000 Spectrophotometer (Thermo Fisher Scientific) to measure absorbance. RNA purity was assessed by observing the 260/280 and 260/230 ratios, which respectively reflect the extent of contamination by proteins and organic compounds, including phenol and guanidinium thiocyanate. It is ideal for RNA samples to have 260/280 ≥ 1.8 and 260/230 ≥ 1.5. However, when working with low amounts of RNA like those from pull-down experiments, concentration (pg/µl) and integrity were determined using the Agilent 2100 Bioanalyzer on the RNA 6000 Pico LabChip (Agilent Technologies). Microfluidic channels in the chip allow for the separation of nucleic acid fragments by size via electrophoresis. After priming the chip with indicated amounts of the gel-

dye mix, RNA marker, and RNA ladder, 1 µl of denatured RNA was loaded into specific wells. The chip was vortexed at 2,400 rpm for 1 min before running the program. Each sample is assigned an RNA integrity number (RIN), which can range from 1 (degraded) to 10 (intact).

3.14 RNA preparation and sequencing

RNA samples were purified using the Clean & Concentrator-5 Kit (Zymo Research), where silica membrane spin columns enable the selective binding and recovery of small and large RNAs (> 17 nt). The procedure involves adding chaotropic salt-based binding buffer and 100% ethanol to samples at RT with wash steps and DNase treatment in between, eventually leading to the elution of ultra-pure RNA using RNase-free water. The rest of the preparation was completed at UC Davis Genome Center. Once ribosomal RNA (rRNA) sequences were depleted with the QIAseq FastSelect HMR Kit (Qiagen), RNA-seq libraries were constructed with the KAPA RNA HyperPrep Kit (Roche). Briefly, whole transcriptome-enriched mRNA was fragmented and transformed into cDNA, which undergoes adaptor ligation, purification, and PCR amplification. Libraries were then loaded onto a flow cell to generate clusters and prepare templates for sequencing, where incorporated bases are detected one by one via fluorescence. Pair-end (PE) sequencing (2x150 bp), which results in more accurate read alignments compared to single-end (SE) sequencing, was performed to an average depth of 30 M reads/sample on the NovaSeq 6000 platform (Illumina).

3.15 Sequence alignment and transcriptome assembly

FASTQ files were forwarded to LC Sciences in Houston, Texas for bioinformatics analysis. After assessing their quality with the FastQC tool, Cutadapt and Perl scripts software

were used to remove reads with adaptor contamination or low-quality and indeterminable bases. With HISAT2, PE reads from each sample were aligned to the *Mus musculus* genome (v101) obtained from Ensembl. Mapped reads of each sample were then assembled using StringTie. With Perl scripts and GffCompare, transcriptomes from all samples in biological triplicate (except one) were merged to reconstruct a comprehensive transcriptome. StringTie and Ballgown were used to quantify transcript expression levels. Transcripts < 200 nt with a Coding Potential Calculator (CPC) score < 0.5 and a Coding-Non-Coding Index (CNCI) score < 0 were discarded. The remaining transcripts were thus identified as lncRNAs.

3.16 Differential expression analysis

StringTie was used to quantify expressed transcripts by calculating fragments per kilobase of transcript per million mapped reads (FPKM). This accounts for the data normalization prior to sample comparison, as FPKM = number of fragments mapped to gene × 10^3 × 10^6 / total number of mapped fragments mapped to genome sequence × gene length (bp). With R packages DESeq2 and edgeR, differentially expressed (DE) transcripts were selected with a $\log_2$(fold change) > 1 or < -1 and a false discovery rate (FDR) < 0.05. The following criteria were used to identify key lncRNAs when comparing samples pulled down by *Ripk1*-targeting BASOs to non-targeted samples: (i) upregulated with $\log_2$(fold change) > 1; (ii) significant with p-value < 0.05; (iii) transcript in *Ripk1*-targeted sample is well-expressed with FPKM > 1; (iv) transcript is neither well-expressed (FPKM ≈ 0) in the non-targeted sample with the same treatment nor the *Ripk1*-targeted sample without treatment. Any known lncRNA sequences of interest were retrieved from the LNCipedia database.

3.17 GapmeR transfections

Macrophages (1-2×10^6 cells/well) were seeded in 6-well plates and maintained in 2 ml of antibiotic-free DMEM media supplemented with 10% FBS. Before transfecting, cells were washed with warm 1x PBS. Opti-MEM (Gibco) and Lipofectamine RNAiMAX (Invitrogen) were used to transfect cells with antisense locked nucleic acid (LNA) GapmeRs (Qiagen). Each lncRNA was expected to be knocked down by a custom-made gapmeR, while Negative Control A was expected to generate non-sequence-specific effects. These gapmeR sequences were designed to complementarily bind select lncRNAs and cause RNase H-mediated degradation. Negative Control A (5' AACACGTCTATACGC 3') was structurally similar to other gapmeRs, but not homologous to any known RNA sequences in the mouse. All gapmeRs and qPCR primers for the lncRNAs of interest are detailed in **Tables S3-S4**. At 6 h and 24 h post-transfection with gapmeRs at a concentration of 50 nM, LPS +/- zVAD treatments were administered for another 6 h before collecting samples for qPCR and western blot analysis. At 12 h, DMEM containing 20% FBS and 2% P/S was added to optimize the 24 h transfection and restore conditions for cell growth.

3.18 Statistical analyses

Data are presented as mean ± standard error of the mean (SEM) or standard deviation (SD) of three independent experiments or a single representative experiment performed multiple times. Statistical analyses were completed on GraphPad Prism 8 software. Comparisons between multiple experimental groups were compared using a two-way analysis of variance (ANOVA). Statistical significance is indicated by the following p-value thresholds: *$p<0.05$, **$p<0.01$, ***$p<0.001$, and ****$p<0.0001$.

4.0 RESULTS

4.1 Establishing inflammatory and necroptotic conditions in macrophages

4.1.1 Increased *Ripk1* and *Tnfa* expression in inflammation and necroptosis

To establish conditions of interest in RAW 264.7 macrophages, these cells were treated with inflammatory stimulus LPS +/- caspase inhibitor zVAD at different times. *Ripk1* expression was analyzed by qPCR at 6 h and 10 h (**Figure 4)**. Differences between the treatments were not statistically significant at 6 h. However, LPS + zVAD treatment after 10 h resulted in the greatest and most significant increase ($p=0.0055$) in *Ripk1* expression. *Ripk1* was also more highly expressed ($p=0.0459$) in LPS-treated samples compared to the no treatment (NT) group.

Commonly used for studying inflammation, LPS not only implicates pathway regulation by RIPK1 but also the synthesis of pro-inflammatory cytokines like TNF-α. We also experimented with TNF-α +/- zVAD treatments, but the resulting *Ripk1* and *Tnfa* expressions were much less prominent (data not shown). However, *Tnfa* expression was examined at the 6 h and 10 h time points (**Figure 5**). It was interesting to see *Tnfa* expression at 6 h increase approximately 15-fold for LPS treatment and 30-fold for LPS + zVAD compared to the NT group. These effects were markedly attenuated at 10 h. Together, the results suggest that LPS does promote TNF-α production in macrophages, but the peak of this process happens relatively early. Unlike what was seen for *Ripk1*, longer LPS exposure does not directly correlate to higher *Tnfa* expression.

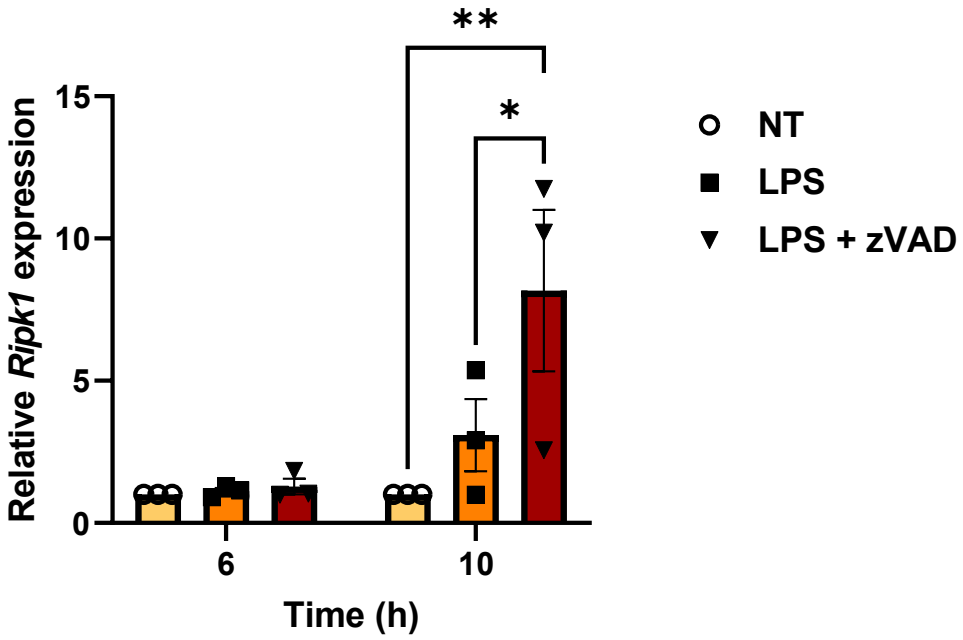

Figure 4. *Ripk1* upregulation in macrophages occurs later in inflammation and necroptosis. Cells were treated with 100 ng/ml LPS +/- 50 μM zVAD. RNA was extracted after 6 h and 10 h for qPCR analysis of *Ripk1* expression. Results are expressed as fold change compared to the NT control. Data points show mean ± SEM, n=3 independent experiments. Statistical significance was analyzed by two-way ANOVA and Šidák's multiple comparison test, *p<0.05, **p<0.01.

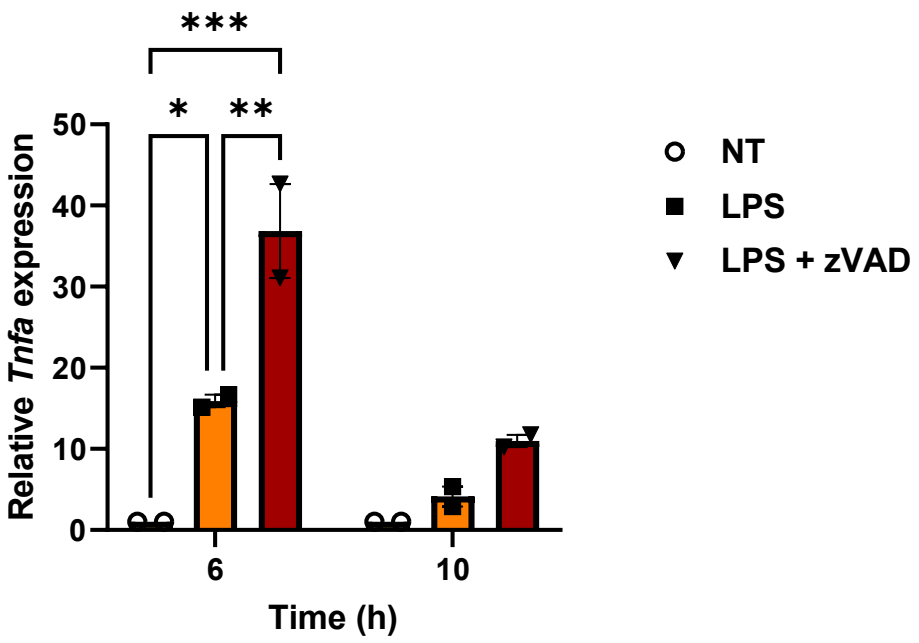

Figure 5. *Tnfa* upregulation occurs earlier in inflammation and necroptosis. Cells were treated with 100 ng/ml LPS +/- 50 μM zVAD. RNA was collected after 6 h and 10 h for qPCR analysis of *Tnfa* expression. Values are displayed as fold change relative to the NT group. Data points display mean ± SEM, n=2 independent experiments.

Given that *Ripk*1 is our mRNA of interest and these findings correlate with previous research indicating its high expression in inflammatory bone marrow-derived macrophages (BMDMs) (25), we deemed the 10 h time point as appropriate for upcoming RAW 264.7 cell treatments with LPS +/- zVAD to induce inflammation and necroptosis.

4.1.2 Dying macrophages exhibit morphological changes

Following LPS +/- zVAD treatments, cultured macrophages were examined under a microscope for changes in their appearance and abundance. NT cells at the 0 h and 10 h time points were mostly round and crowded together (**Figure 6A-B**). In contrast, LPS-treated cells were more spread out after 10 h, likely in response to the inflammatory environment (**Figure 6C**). Macrophages stayed elongated in the presence of both LPS and zVAD, although at a visibly lower density because necroptotic cells no longer adhere to the plate (**Figure 6D**). Such patterns were likewise seen at the 6 h time point, but to a lesser extent (data not shown).

Cytotoxicity assays were done to measure the amount of macrophage death under different conditions. While LDH release in LPS-stimulated samples does not differ considerably from that in NT controls, around a 6-fold difference was observed in macrophages treated with LPS + zVAD for 6 h, and slightly over 6.5-fold for 10 h (**Figure 7**). This further supports that necroptosis is taking place, as cell membrane disruption is a prerequisite to LDH release into the media.

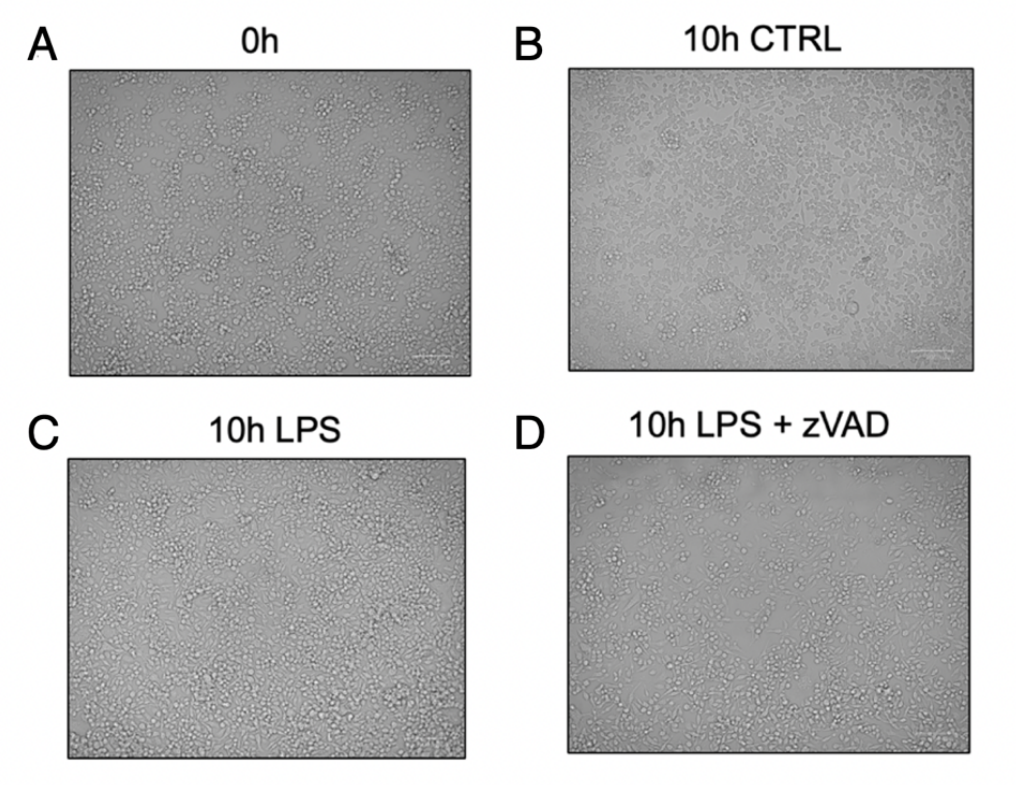

Figure 6. Macrophage morphology changes during inflammation and necroptosis. RAW 264.7 cells were visualized under a microscope after 0 h (**A**) and 10 h (**B**) time points, representing the controls. Changes in cell quantity and morphology were observed in wells treated with LPS to induce inflammation (**C**), and LPS + zVAD to induce necroptosis (**D**).

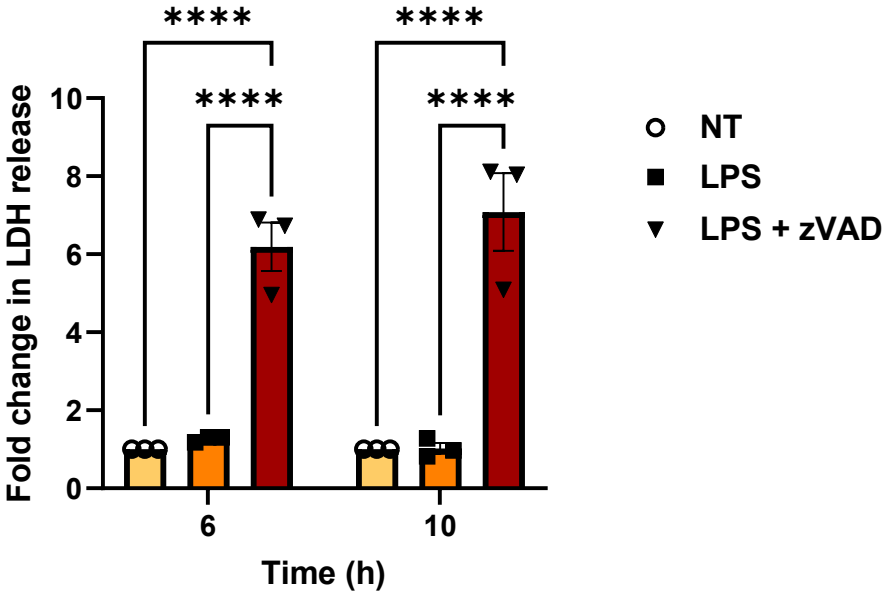

Figure 7. Significant cell death in macrophages treated with LPS + zVAD. Macrophages were treated with LPS +/- zVAD for 6 h and 10 h before collecting samples for cytotoxicity assays. As LDH release due to plasma membrane rupture catalyzes NADH oxidation, changes in absorbance at 340 nm were recorded to measure the reaction rate. Fold change was calculated by comparing to the NT control. Results are expressed as mean ± SEM, n=3 independent experiments. Statistical significance was analyzed by two-way ANOVA and Tukey's multiple comparison test, ****$p<0.0001$.

4.2 Half-life determination of *Ripk1* mRNA and RIPK1 protein

4.2.1 *Ripk1* mRNA turnover

To learn more about the post-transcriptional regulatory mechanisms of RIPK1, we studied its mRNA stability in macrophages under normal and inflammatory conditions. This involved carrying out mRNA decay assays with Actinomycin D (ActD), which binds DNA at the transcription initiation complex to prevent RNA polymerase from extending the chain. Stopping new mRNA synthesis helps to reveal how long existing *Ripk1* mRNA lasts inside the cell, as changes in its expression are monitored by qPCR.

Figure 8A shows how much *Ripk1* mRNA expression deviates from starting levels at 0 h in macrophages with NT or ActD alone. Since many genes upregulate or downregulate in response to new stimuli, it is logical that *Ripk1* mRNA levels in cells with NT do not change drastically over time. This NT condition thus represents steady-state *Ripk1* mRNA levels, as determined by the rates of transcript synthesis and decay. However, changes in *Ripk1* mRNA expression were far more obvious in cells treated with ActD. This decline in *Ripk1* transcript abundance corresponds to an approximate half-life of 3.33 h in macrophages under normal conditions.

Next, we investigated whether these trends in *Ripk1* mRNA expression are altered by simultaneously adding LPS to cause inflammation (**Figure 8B**). Although some fluctuation is expected and apparent in cells stimulated by LPS alone, *Ripk1* mRNA levels at 4 h were still close to those at 0 h. Compared to the data for the NT condition above, *Ripk1* mRNA decay did not differ greatly in macrophages treated with LPS at the same time as ActD. By 4 h, both NT and

LPS groups with ActD showed *Ripk1* mRNA levels falling to about 40% of what was originally present at 0 h. *Ripk1* mRNA half-life for this LPS + ActD co-treatment was averaged to be 3.49 h.

In contrast to the previous findings, *Ripk1* mRNA expression in macrophages pre-treated with LPS for 10 h persisted in both the absence and presence of ActD (**Figure 8C**). Over the course of 4 h, the percentages of remaining *Ripk1* transcript were similar for both groups. This reduction in *Ripk1* mRNA decay or enhancement in its stability may be due to various molecular modifications occurring in inflammatory macrophages. While we did not determine the *Ripk1* transcript half-life given the similar levels across the set time points, it is evidently extended by the prolonged exposure to LPS.

Altogether, the results suggest that *Ripk1* mRNA is being made and turned over regularly in macrophages. The transcript half-life hovers around a few hours, which is short in comparison to most mRNAs (67). Furthermore, it can depend on the timing and duration of LPS-induced inflammation. Co-treating macrophages with LPS + ActD does not lead to substantial changes in *Ripk1* mRNA decay compared to treating with ActD only. However, pre-treating cells with LPS for 10 h before inhibiting transcription leads to increased *Ripk1* mRNA stability. These observations ultimately contribute to the understanding of how post-transcriptional control for *Ripk1* can be altered by macrophage inflammation.

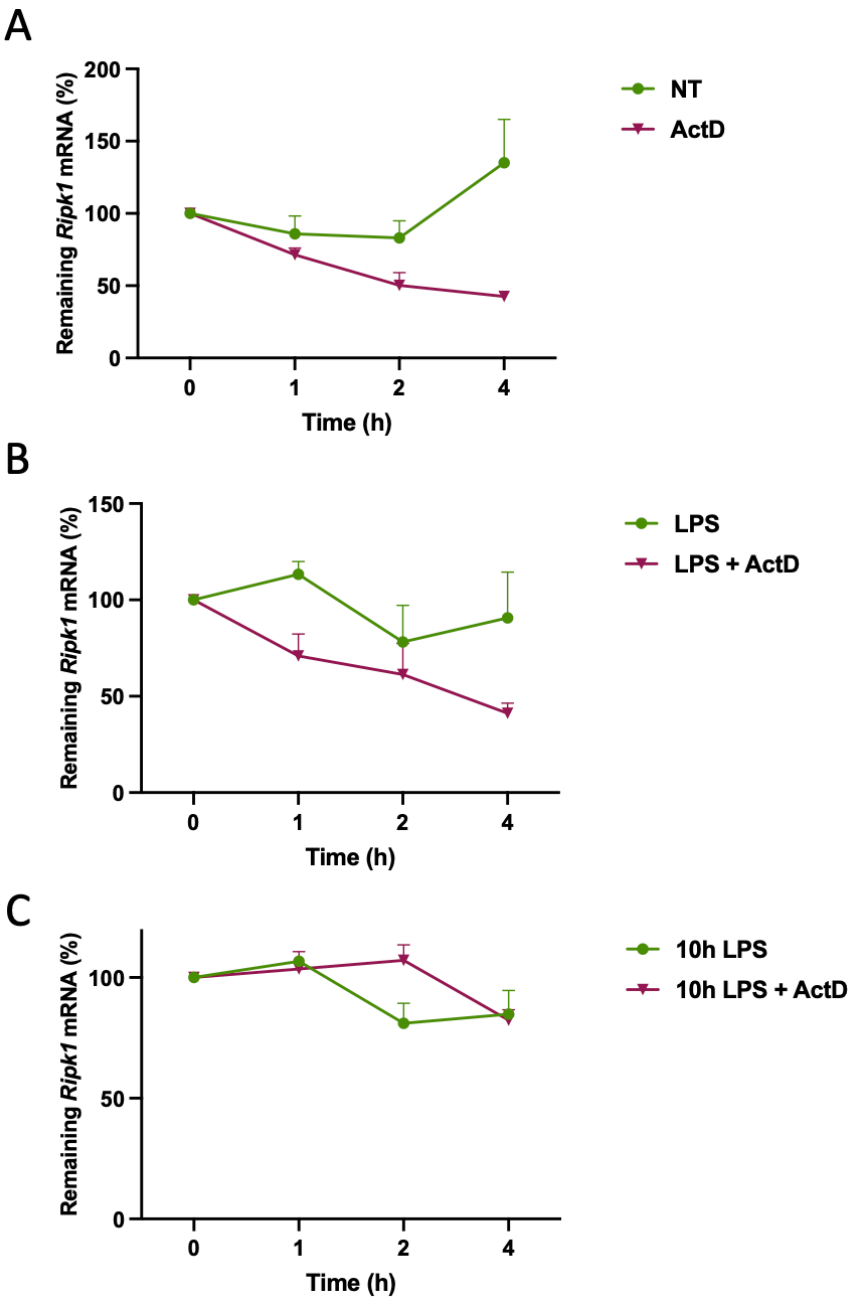

Figure 8. Increased *Ripk1* mRNA stability in macrophages pre-treated with LPS. Before adding 10 µg/ml ActD and extracting RNA at 0, 1, 2, and 4 h, cells were either left with NT (**A**), co-treated with 100 ng/ml LPS at 0 h (**B**), or pre-treated with LPS for 10 h (**C**). *Ripk1* mRNA levels were quantified by qPCR and normalized to *Srp14*. Percentages of the remaining *Ripk1* transcript were plotted for each scenario. Data show mean ± SEM, n=3 independent experiments.

4.2.2 RIPK1 protein turnover

Considering the inextricable link between transcription and translation, the other topic of investigation was protein stability. RIPK1 turnover was monitored in macrophages under the same LPS conditions as the mRNA decay assays but using cycloheximide (CHX) instead. CHX is a chemical that binds eukaryotic ribosomes to block the translocation step of protein synthesis, thereby allowing us to examine the rate at which RIPK1 degrades more accurately.

In NT cells, RIPK1 protein expression appeared to fluctuate to some extent over time (**Figure 9A-B**). Such decreases in expression are likely detected by cells and then replenished by ongoing translation. On the flipside, CHX treatment led to a greater decline in RIPK1 by 9 h. After quantifying band intensities and plotting data points, we determined the RIPK1 protein half-life to be 3.09 h by linear regression. This is relatively short compared to most proteins (68), suggesting that RIPK1 is turned over regularly in macrophages.

When cells were treated with LPS only, we observed a similar trend to NT cells where RIPK1 protein expression dipped slightly at 3 h but rose back gradually by 9 h (**Figure 9C-D**). Co-treatment of LPS and CHX showed upregulated RIPK1 levels around 3 h, which was followed by a sharp decrease before 6 h and 9 h. The corresponding blot shows a noticeable disappearance of the RIPK1 band at these later time points. Under these LPS + CHX treatment conditions, we calculated the RIPK1 protein half-life to be 3.07 h, which virtually does not differ from the original half-life under NT conditions.

Since our previous qPCR analyses established *Ripk1* upregulation in LPS-treated cells, we sought to study how such prolonged inflammatory conditions affect the protein half-life. We administered LPS for 10 h and removed the treatment before starting the CHX time course (**Figure**

9E-F). RIPK1 expression in cells pre-treated with LPS seemed stable between 0 h and 6 h of being in regular media but increased from 6 h to 9 h. However, RIPK1 levels dropped steadily when CHX was added. Unlike the previous two CHX-induced patterns, LPS pre-treatment helped slow down RIPK1 degradation by increasing its expression and stability. This is reflected by its extended half-life, which we calculated to be 5.11 h.

In general, protein turnover is a relevant facet of gene expression control that varies depending on different cellular conditions. From these results, we can conclude that RIPK1 under normal conditions is quite unstable with a short half-life of approximately 3 h. This does not change when cells are treated with LPS at the same time as CHX. However, RIPK1 half-life and stability in macrophages can be extended by prolonged exposure to LPS before beginning the CHX chase assay. Half-life determination of *Ripk1* mRNA and RIPK1 protein in macrophages subject to normal and inflammatory conditions are presented below (**Table 1**).

Table 1. mRNA and protein half-lives for RIPK1 in macrophages with or without LPS treatments.

Half-life	No treatment	LPS co-treatment	10h LPS pre-treatment
mRNA	3.33 h	3.49 h	n/a
protein	3.09 h	3.07 h	5.11 h

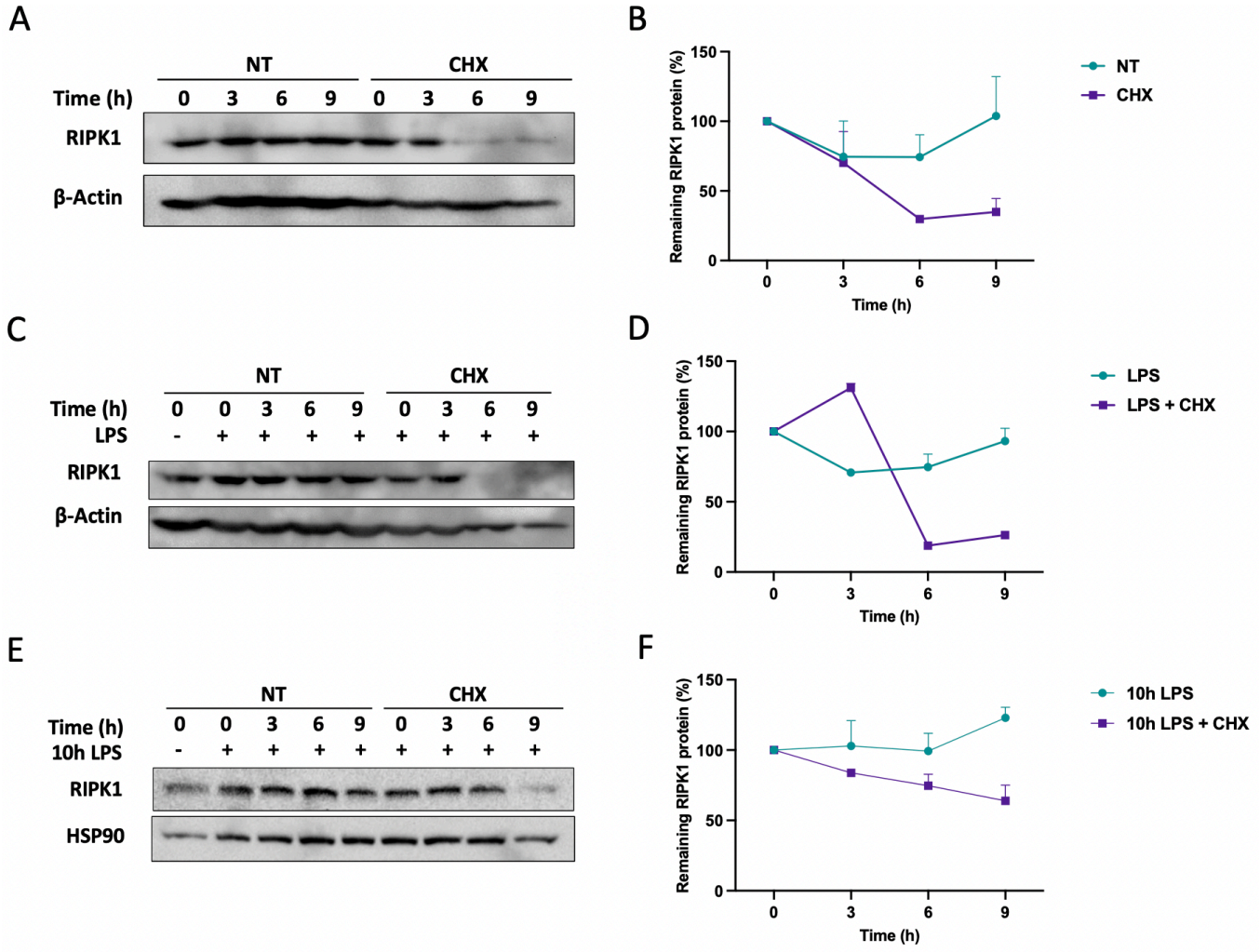

Figure 9. RIPK1 protein stability increases in macrophages pre-treated with LPS. Cells were either treated with 20 µg/ml CHX (**A-B**) or simultaneously treated with 100 ng/ml LPS and CHX (**C-D**) for 0, 3, 6, and 9 h. Alternatively, cells were pre-treated with LPS for 10 h (**E-F**) before conducting CHX chase assays and collecting samples at the indicated times for protein analysis. RIPK1 expression was quantified and normalized to β-actin or HSP90 before remaining levels relative to 0 h were determined for each control and treatment condition. Western blots are representative of n=2 independent experiments. Corresponding line graphs illustrate mean percentage ± SEM.

4.3 Optimization of RNA pull-down experiments

4.3.1 Design and validation of ASOs binding *Ripk1* mRNA

Prior to designing complementary ASO sequences that target *Ripk1* mRNA, we visited the Ensembl database to retrieve the mature *Ripk1* mRNA transcript, which includes 11 exons flanked by 3' and 5' UTRs on each end. Uploading this sequence onto the RNAfold web server allowed us to visualize *Ripk1* mRNA's secondary structure, which consists of many stems, loops, and branches (**Figure 10A**). To maximize the ease and likelihood of capturing *Ripk1* mRNA, we selected multiple target regions with low steric hindrance spread across different exon-exon junctions and the 3' UTR, one of which is pictured in **Figure 10B**.

Once the ASOs were ready, we evaluated their capacity to bind *Ripk1* mRNA by comparing gene expression levels in samples with an individual ASO added to those without. When an ASO is present and functioning as expected, *Ripk1* expression is lower compared to samples without the ASO. This possibly occurs because the ASO interferes with the qPCR primers' ability to detect the target region. Adding RNase H, which degrades the RNA where the ASO is bound to form a DNA-RNA hybrid (**Figure 11A**), supports this interaction by further lowering *Ripk1* expression. Data is displayed for one ASO that targets the 3' UTR in **Figure 11B**, and another ASO targeting the exon 8-exon 9 junction in **Figure 11C**. In total, six ASOs were successfully validated for their ability to target *Ripk1* mRNA. Their sequences are presented in **Table S1**.

Figure 10. Predicted secondary structure of *Ripk1* mRNA. After obtaining the mature transcript from the Ensembl genome browser, *Ripk1* mRNA was visualized on the RNAfold web server to design custom ASOs (**A**). This enables the selection of areas on the mRNA with lower steric hindrance for better ASO binding, such as this highlighted target sequence in the 3' UTR (**B**).

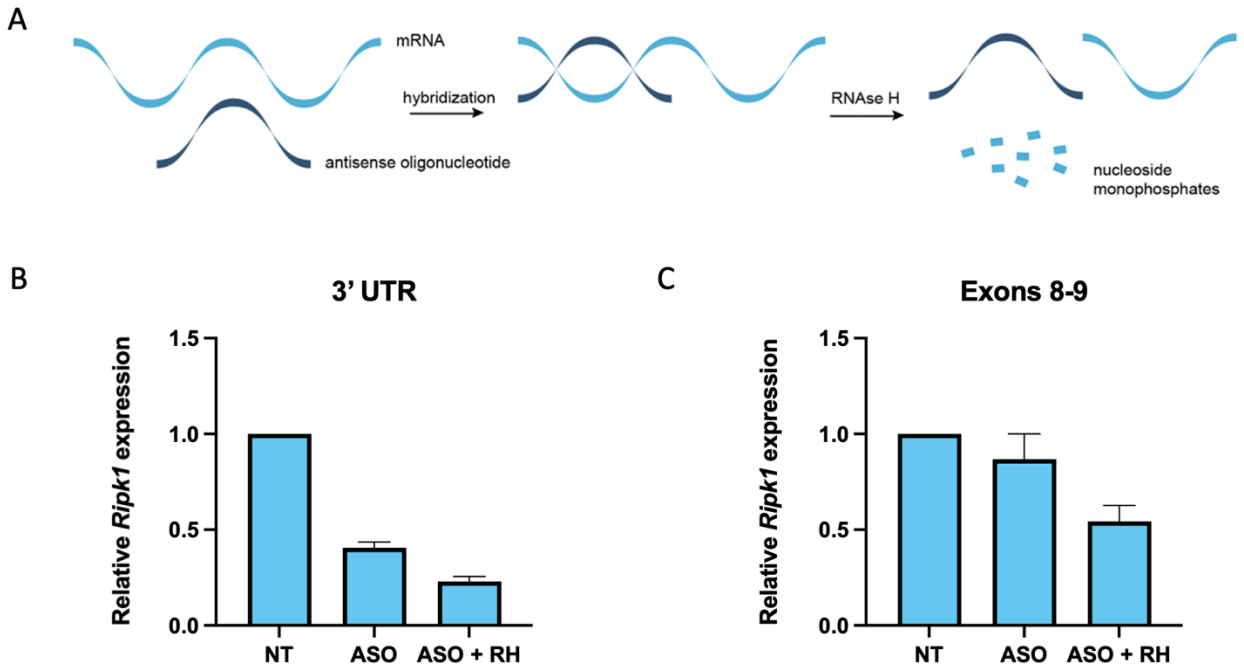

Figure 11. Decreased qPCR detection due to ASOs binding *Ripk1* mRNA. (A) Binding validation assays involved combining individual ASOs +/- RNase H (RH) with cell lysates. Functional ASOs are expected to hybridize with *Ripk1* mRNA before RNase H selectively degrades the RNA in this DNA-RNA hybrid. Relative *Ripk1* expression was quantified by qPCR for one ASO targeting the 3' UTR (**B**) and another targeting the exon 8-exon 9 junction (**C**). Results are shown as fold change relative to the NT control. Error bars are ± SD, n=3 technical replicates.

4.3.2 Verification of *Ripk1* expression in pulled-down RNA

Biotinylated versions of validated ASOs, along with a scrambled control, were incorporated into our pull-down experiments to capture *Ripk1* mRNA and attaching lncRNAs. As illustrated in **Figure 12**, the workflow involves combining macrophage lysates with biotinylated ASOs (BASOs) and streptavidin magnetic beads, as well as incubation and wash steps in between. Total RNA isolation was then performed before processing the samples for sequencing.

For macrophages with NT, we also compared *Ripk*1 expression in samples with *Ripk1*-targeting BASOs to those with the non-targeting BASO. Since pulled-down RNA samples were lowly concentrated according to spectrophotometer measurements and undetectable by regular qPCR, we resorted to droplet digital PCR (ddPCR). This latter technology differs from its more common counterpart by focusing on absolute instead of relative nucleic acid quantification. It is also known for having higher precision, which is preferred for low input target concentrations.

As seen in **Figure 13**, ddPCR revealed extremely low copies of *Ripk1*. Although the *Ripk1*-specific BASOs yielded 1.73 copies/µl, which was marginally more than 0.74 copies/µl in the scrambled BASO group, the difference between the two failed to yield statistical significance ($p=0.4286$). However, the presence of *Ripk1* and its relatively higher expression in the *Ripk1*-binding BASO group still encouraged us to proceed with pulling down RNA from LPS +/- zVAD-treated macrophages for sequencing, while being aware of the low amounts we were working with.

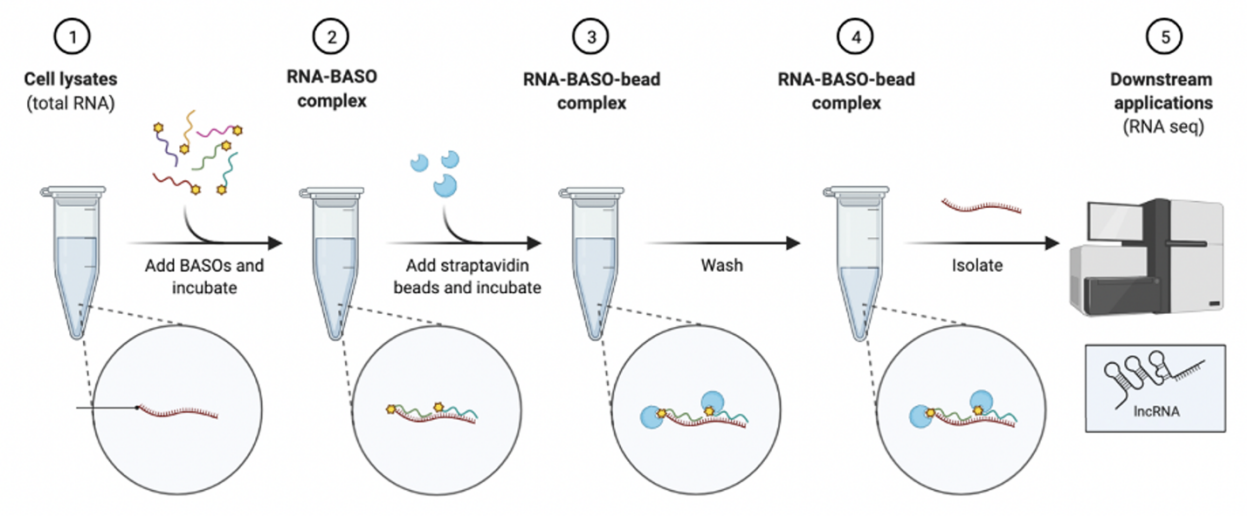

Figure 12. Workflow for RNA pull-down experiments. Biotinylated ASOs (BASOs) and streptavidin magnetic beads were used to pull down *Ripk1* mRNA with its attaching lncRNAs from RAW 264.7 cells, which were either untreated or treated with LPS +/- zVAD for 10 h. Once isolated and purified, RNA samples were prepared for sequencing and analysis.

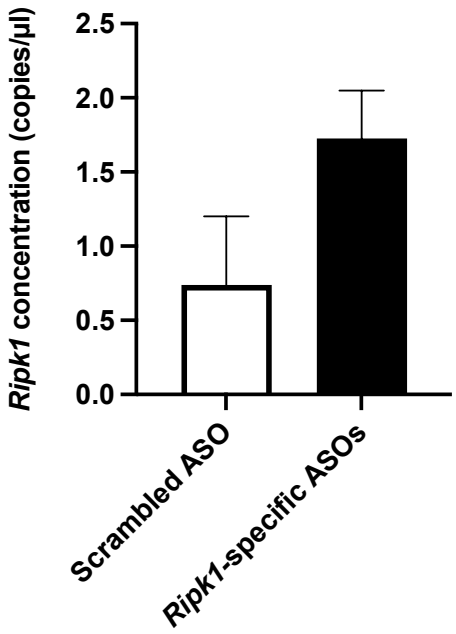

Figure 13. Low droplet digital PCR detection of *Ripk1* in pulled-down RNA samples. Cell lysate preparations treated with *Ripk1*-targeting BASOs were compared to those with a scrambled control BASO sequence. Absolute concentrations (copies/µl) of *Ripk1* were generated by QuantaSoft software. Data represent mean ± SEM, n=2 independent experiments.

4.3.3 Assessment of pulled-down RNA quality

To check whether the quality of our pulled-down RNA was sufficient for sequencing, we ran each sample on the Bioanalyzer to measure concentration and integrity. Results for assessing integrity from one independent round of RNA pull-downs (6 samples) are depicted in **Figure 14A**. Samples were assigned high RNA integrity numbers (RINs) between 8.20 and 9.50, corresponding to electropherograms that feature sharp ribosomal peaks and low background noise.

Figure 14B shows Bioanalyzer data for these same samples after passing them down spin columns for cleaning and treating with DNase, the final recommended step before sequencing. Some RNA was lost in the process since final concentrations for the 18 samples were lower than before purification, ranging from 3 to 35 pg/µl (data not shown). The ribosomal peaks also became much smaller in size. Unexpectedly, RNA quality did not appear to improve, given the lower RINs between 3.90 and 8.60. This may be due to several reasons, including the relatively lengthy (15 min) exposure to DNase at RT and imperfect Bioanalyzer assessment of low RNA quantities (69).

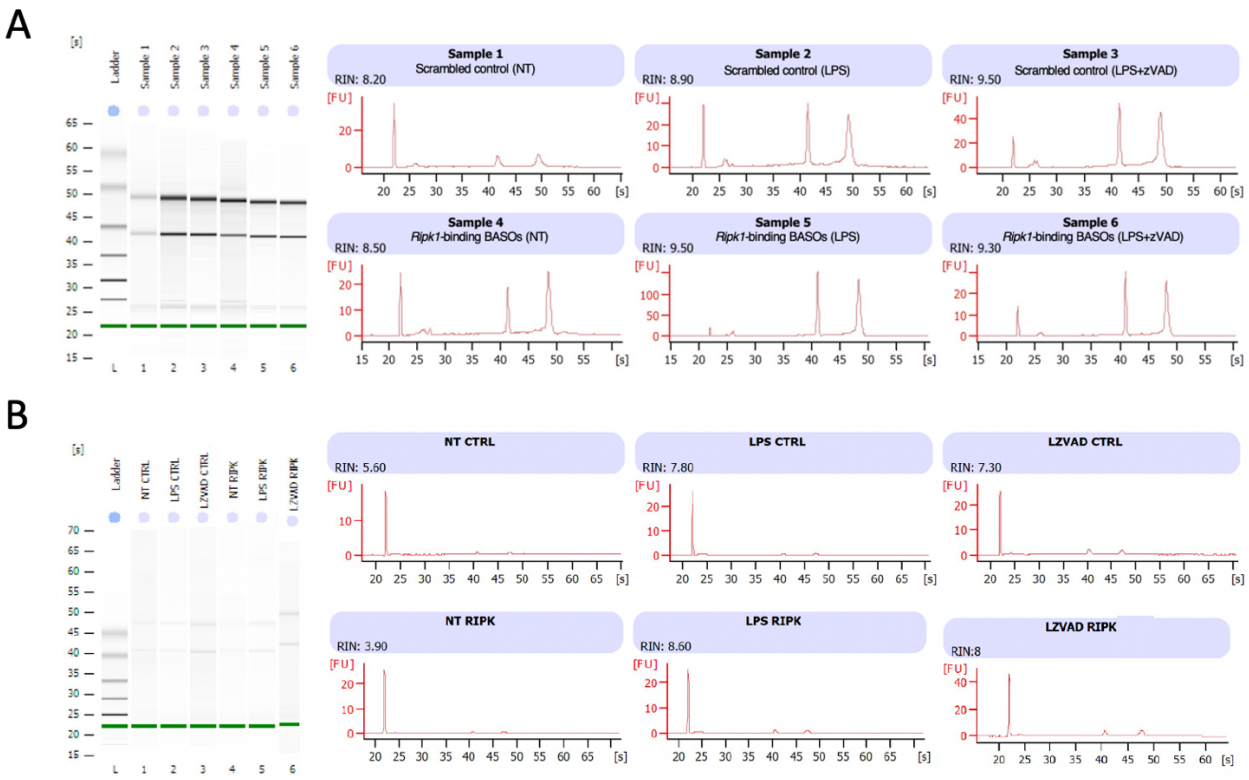

Figure 14. Pulled-down RNA remains intact with ribosomal RNA present. Bioanalyzer outputs for each RNA sample include a gel-like image and an electropherogram. Total RNA was isolated from NT or LPS +/- zVAD-treated macrophages, lysed and combined with either one scrambled control BASO or six *Ripk1*-binding BASOs. Each sample is assigned an RNA integrity number (RIN), which can range from 1 (degraded) to 10 (intact). Assessments were performed before (**A**) and after (**B**) spin-column purification and DNase treatment. Data are representative of n=3 independent experiments.

4.4 Sequencing and analysis of lncRNAs in *Ripk1*-targeted pull-downs

4.4.1 Overview of samples and read variability

The bioinformatics pipeline for lncRNA sequencing is outlined in **Figure 15**. Briefly, raw data files were cleaned, and reads were mapped to the *Mus musculus* reference genome before transcript assembly and expression profiling. Known lncRNAs were annotated, while novel lncRNAs were discovered upon filtering by nt length and coding potential.

Principal component analysis (PCA) reduces the dimensionality of complex datasets to visualize major directions of sample variability. Looking at **Figure 16A,** there is no outstanding discrimination across different sample types. Although, this is not unusual and can largely depend on the effect size and underlying biological noise. While it is not always expected for biological replicates to cluster, pulled-down RNA from the first and third rounds of our experiments appear to be more similar. In contrast, samples in the second set are plotted farther away and amongst themselves, showing greater variability in gene expression profiles.

Box plots were also generated to visualize the distribution of transcript expression for each sample. These levels were represented by log10(FPKM) values, which allow for within-sample normalization (70). Unlike raw read counts, FPKM accounts for factors such as varying transcript lengths, read numbers, and sequencing biases (70). In **Figure 16B,** we can see similar distributions in the normalized data, setting the stage for inter-sample comparisons. Information on the range of expression levels across samples is further relevant for determining acceptable FPKM threshold values for differential expression (DE) analysis.

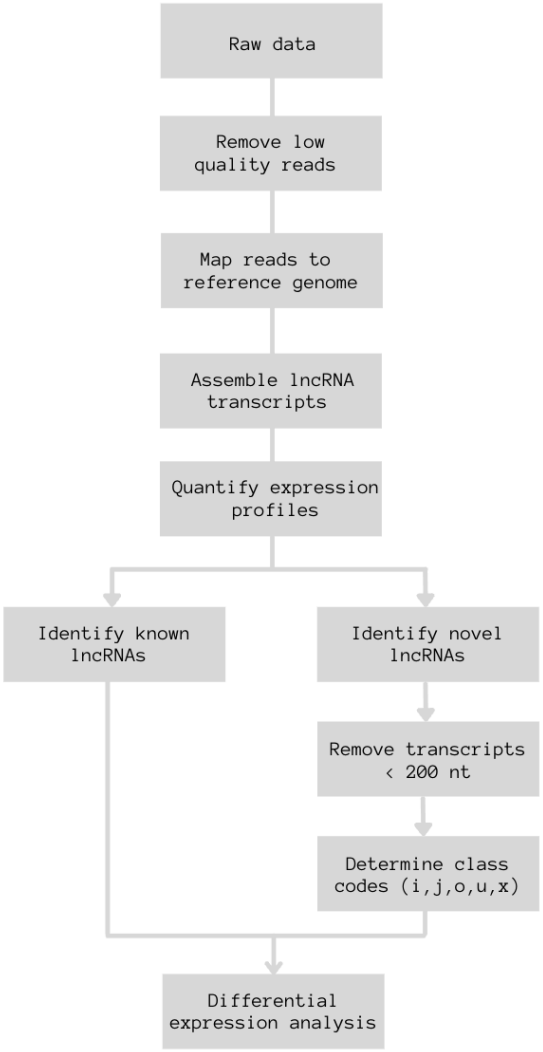

Figure 15. Bioinformatics pipeline for lncRNA sequencing. Quality control, genome mapping, transcripts assembly, and sequencing analysis services were provided by LC Sciences. These steps are further detailed in the methods section.

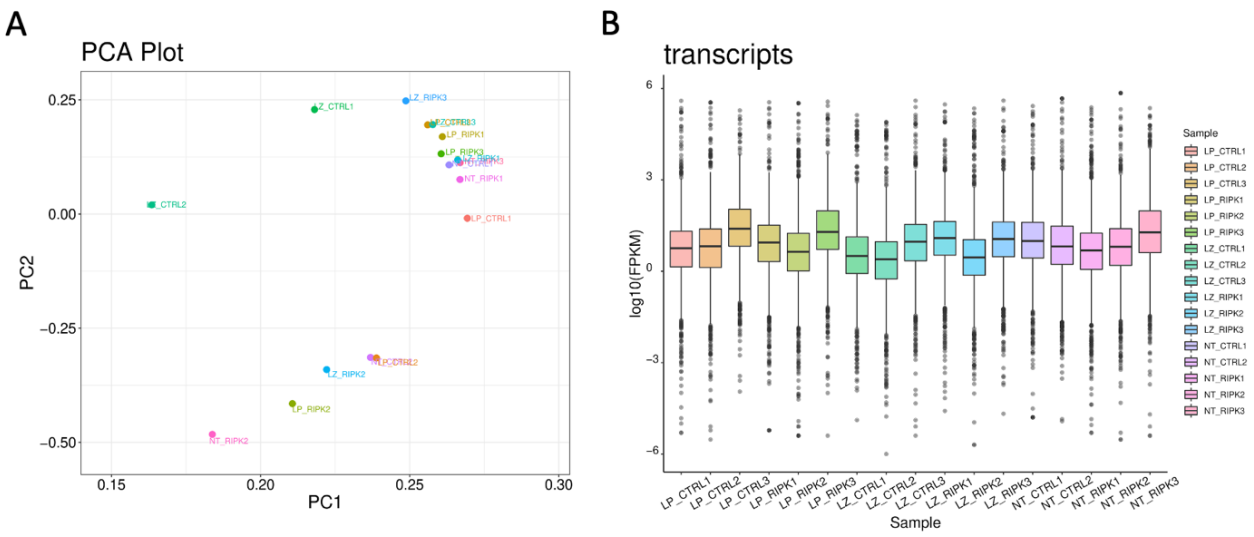

Figure 16. Similarity analyses of RNA sequencing data. (A) Principal component analysis depicts the variability between biological replicates. This plot reduces the dimensionality of complex datasets to principal components PC1 and PC2. Points represent different samples (NT, LP=LPS, LZ=LPS + zVAD treatments; RIPK and CTRL ASOs), where replicates are numbered 1, 2, or 3. Samples with similar gene expression profiles cluster together. **(B)** Box plots illustrate the distribution of transcript expression in each sample. Higher log10(FPKM) values on the y-axis correspond to more abundant gene expression. Horizontal lines on a box and whisker plot refer to five statistics from top to bottom: maximum, upper quartile, median, lower quartile, and minimum.

4.4.2 Differential expression and selection of candidate lncRNAs

To discover lncRNAs in *Ripk1* mRNA-enriched samples, we analyzed DE data by comparing lncRNAs in RIPK samples to CTRLs for each condition (NT, LPS, LPS + zVAD) separately. Because we are primarily interested in *Ripk1*-related lncRNA expression during inflammation and necroptosis, we excluded lncRNAs in the LPS and LPS + zVAD groups that were likewise found in the NT group. These comparisons are illustrated and indicated by arrows in **Figure 17**.

Statistically significant upregulation and relatively high expression were prioritized when developing specific selection criteria to identify lncRNA transcripts of interest (**Figure 18A**). Following DE analysis, we sorted lncRNA data by the highest positive log2(fold change) values with the lowest p-values (<0.05) and relatively high FPKM values (>1) in more than two RIPK replicates. Additionally, it was important for FPKM values in all CTRL replicates to be 0 or < 1 to ensure specificity.

The number of significantly upregulated known and novel lncRNAs for each group is displayed in a Venn diagram (**Figure 18B**). Altogether, we counted 36 *Ripk1*-associated lncRNAs, of which 9 were specific to LPS samples, 25 were specific to LPS + zVAD samples, and 1 was common to both treatments.

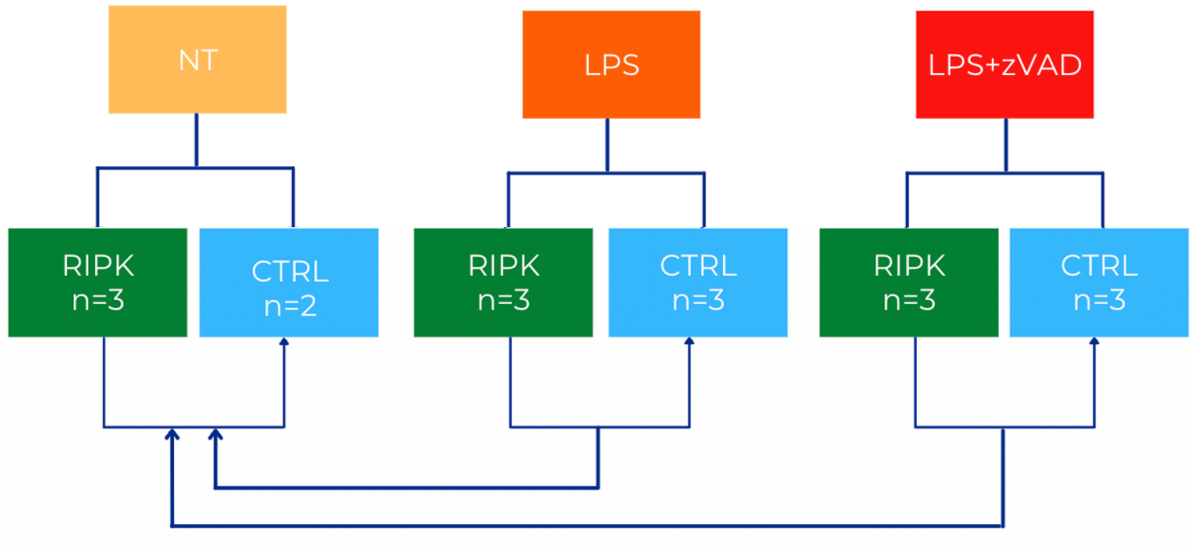

Figure 17. Plan for differential expression analysis and candidate lncRNA selection. The experiment consists of 3 groups: no-treatment (NT), inflammatory LPS, and necroptotic LPS + zVAD. For each treatment, there are two sample types: one with BASOs targeting *Ripk1* mRNA (RIPK), which is compared to the other with a non-targeting BASO sequence (CTRL). Biological triplicates were generated for all samples (n=17), except one due to poor library preparation. Upregulated *Ripk1*-associated lncRNAs in macrophages subject to LPS and LPS + zVAD conditions were subsequently compared to those in the NT group.

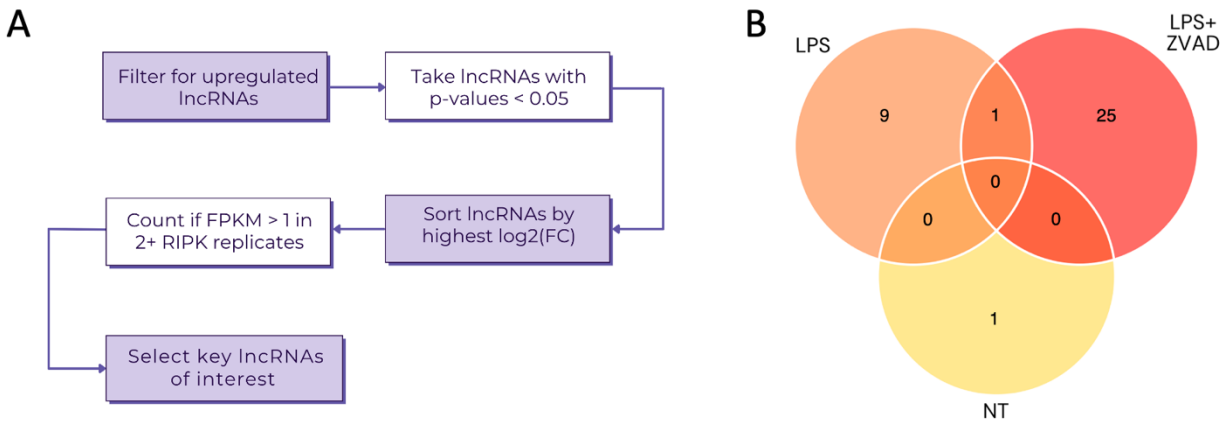

Figure 18. Upregulated lncRNAs in *Ripk1*-targeted samples compared to non-targeted samples. (**A**) Counted lncRNAs are expressed (FPKM > 1) in more than two *Ripk1* mRNA-targeted replicates and not expressed in any corresponding non-targeted replicates, with log2(fold change) values > 1 and p-values < 0.05. (**B**) Yellow, orange, and red circles in this Venn diagram respectively refer to NT, LPS, and LPS + zVAD treatments. Numbers in the overlap between two circles indicate upregulated lncRNAs in both conditions.

Known and novel lncRNAs in the NT condition are listed in descending order of log2(fold change) in **Tables 2A-B**. The top three for each were included here because upregulated lncRNAs were more limited and less significant than the other comparisons. The three known lncRNAs were annotations of the same 923-nt long transcript originating from different locations on chromosome 21. Meanwhile, the three novel lncRNAs had higher fold changes, shorter sequences, and different chromosome locations. Of all the upregulated lncRNAs in *Ripk1*-targeted samples with NT, novel lncRNA MSTRG.7969.1 had the highest log2(fold change) of 19.96 and was also the only one with a p-value < 0.05.

Table 2A. Top 3 known lncRNAs in *Ripk1*-targeted samples with no treatment.

LncRNA	Transcript	Length	Gene ID	Chromosome	log2(fold change)	p-value	q-value
FP671120	ENST00000629969	923	MSTRG.8183	21	4.16	0.16	0.83
FP236383	ENST00000627981	923	MSTRG.8206	21	3.9	0.18	0.87
FP671120	ENST00000631211	923	MSTRG.8171	21	3.84	0.19	0.89

Table 2B. Top 3 novel lncRNAs in *Ripk1*-targeted samples with no treatment. Class codes classify lncRNAs by genomic location: intronic lncRNAs (i); lncRNAs sharing a transcript with at least 1 splice junction (j); exonic lncRNAs overlapping with a transcript (o); intergenic lncRNAs (u).

LncRNA	Class code	Length	Nearby gene	Chromosome	log2(fold change)	p-value	q-value
MSTRG.7969.1	u	202	N/A	20	19.96	0.04	0.55
MSTRG.5209.5	j	249	C16orf87	16	18.18	0.12	0.78
MSTRG.3832.2	o	463	RBM26	13	16.58	0.11	0.77

In *Ripk1*-targeted samples undergoing LPS-induced inflammation, we recorded the top three upregulated known lncRNAs and all the significantly upregulated novel lncRNAs (**Tables 3A-B**). LncRNA AC125611 was chosen for further analysis, as the only known lncRNA upregulated among the LPS group with a p-value < 0.05. Novel lncRNAs MSTRG.5894.1 and MSTRG.5684.5 were also selected for having the lowest p-values, rounding to 0.01. Both are transcribed from chromosome 17 and their nearby genes are ACACA and WSB1, respectively.

Table 3A. Top 3 known lncRNAs in *Ripk1*-targeted samples in LPS-induced inflammation. Asterisk (*) indicates lncRNA is selected for functional validation.

LncRNA	Transcript	Length	Gene ID	Chromosome	log2(fold change)	p-value	q-value
RAB11B-AS1	ENST00000593581	1013	ENSG00000269386	19	15.99	0.05	0.53
ZEB2-AS1	ENST00000427278	2013	MSTRG.7481	2	13.57	0.10	0.58
AC125611*	ENST00000550468	680	MSTRG.3183	12	7.1	0.02	0.27

Table 3B. Novel lncRNAs significantly upregulated in *Ripk1*-targeted samples in inflammation. Class codes classify lncRNAs by genomic location: intronic lncRNAs (i); lncRNAs sharing a transcript with at least 1 splice junction (j); exonic lncRNAs overlapping with a transcript (o); intergenic lncRNAs (u).

LncRNA	Class code	Length	Nearby gene	Chromosome	log2(fold change)	p-value	q-value
MSTRG.5894.1*	i	234	ACACA	17	19.5	0.01	0.1
MSTRG.12587.12	j	275	RNF38	9	18.8	0.02	0.28
MSTRG.2095.1	i	287	LRMDA	10	18.56	0.03	0.31
MSTRG.3830.1	i	281	MYCBP2	13	18.08	0.04	0.47
MSTRG.5684.5*	j	915	WSB1	17	17.84	0.01	0.17
MSTRG.10721.1	o	351	AL031777	6	17.02	0.05	0.51
MSTRG.5866.4	j	941	TAF15	17	16.86	0.03	0.3
MSTRG.7811.17	j	639	CUL3	2	7.44	0.02	0.22

MSTRG.5684.5 further piques our interest because it was even more highly and significantly upregulated in the LPS + zVAD category, with an adjusted p-value or q-value of 0.04. The other novel lncRNA MSTRG.7477.1 with ZEB2 as its nearby gene was significantly upregulated to a similar extent and additionally selected for manipulation in subsequent experiments. Information on the other known and novel lncRNAs upregulated in necroptosis is presented in **Tables 4A-B**. No known lncRNAs were chosen for functional validation here, mainly because FPKM values were low (data not shown) and nearing our set threshold. We remarked well-known lncRNA metastasis-associated lung adenocarcinoma transcript 1 (MALAT1) to be among this group, although its expression was still limited, and its fold change was not significant.

In summary, four lncRNAs with consistently high expression and the most significant upregulation were chosen for functional validation and secondary structure prediction (**Figure 19**). Their average FPKM values in replicates with *Ripk1*-specific BASOs ranged from 35.2 to 79.3, while log2(fold change) values were between 7.1 and 19.5. Known lncRNA AC125611 and novel lncRNA MSTRG.5894.1 were linked to LPS-induced inflammation, novel lncRNA MSTRG.7477.1 was linked to LPS + zVAD-induced necroptosis, and novel lncRNA MSTRG.5684.5 was linked to both treatment conditions.

Table 4A. Top 3 known lncRNAs in *Ripk1*-targeted samples in LPS + zVAD-induced necroptosis.

LncRNA	Transcript	Length	Gene ID	Chromosome	log2(fold change)	p-value	q-value
AC009299	ENST00000652531	1028	MSTRG.7527	2	15.98	0.04	0.58
MALAT1	ENST00000534336	8708	ENSG00000251562	11	3.91	0.20	0.65
TMEM202-AS1	ENST00000565181	2325	MSTRG.4756	15	3.62	0.26	0.73

Table 4B. Novel lncRNAs significantly upregulated in *Ripk1*-targeted samples in necroptosis. Class codes classify lncRNAs by genomic location: intronic lncRNAs (i); lncRNAs sharing a transcript with at least 1 splice junction (j); exonic lncRNAs overlapping with a transcript (o); intergenic lncRNAs (u).

LncRNA	Class code	Length	Nearby gene	Chromosome	log2(fold change)	p-value	q-value
MSTRG.12666.1	i	248	ZFAND5	9	19.6	0.01	0.21
MSTRG.7477.1*	i	295	ZEB2	2	19.47	1.7E-03	0.04
MSTRG.6571.1	i	354	ATP9B	18	19.31	0.01	0.15
MSTRG.5684.5*	j	915	WSB1	17	19.01	1.9E-03	0.04
MSTRG.2076.1	i	367	LRMDA	10	18.96	0.02	0.26
MSTRG.7591.1	i	289	MAP3K20	2	18.79	0.02	0.3
MSTRG.7461.1	i	361	ARHGAP15	2	18.74	0.01	0.24
MSTRG.2081.1	i	314	LRMDA	10	18.72	0.02	0.29
MSTRG.8383.6	j	531	HIRA	22	18.46	0.01	0.19
MSTRG.11347.1	i	209	SKAP2	7	18.42	0.04	0.58
MSTRG.12883.1	i	451	DENND1A	9	18.32	0.01	0.25
MSTRG.12882.1	i	337	DENND1A	9	18.28	0.03	0.43
MSTRG.12884.1	i	283	DENND1A	9	18.24	0.03	0.5
MSTRG.12071.1	i	481	ST18	8	18.08	3.1E-03	0.07
MSTRG.2828.1	i	315	CADM1	11	18.04	0.03	0.39
MSTRG.10721.1	o	351	AL031777	6	18.03	0.01	0.25
MSTRG.11568.1	i	382	SLC25A13	7	18.03	0.03	0.47
MSTRG.5285.29	j	377	ATXN2L	16	17.98	0.02	0.36
MSTRG.12595.1	i	244	ZCCHC7	9	17.97	0.04	0.53
MSTRG.11338.1	u	645	N/A	7	17.75	0.02	0.3
MSTRG.2067.1	i	616	LRMDA	10	17.71	0.02	0.32
MSTRG.2092.1	i	304	LRMDA	10	17.7	0.03	0.48
MSTRG.9206.1	i	509	RSRC1	3	17.68	0.02	0.33
MSTRG.9156.4	j	431	TSC22D2	3	17.51	0.05	0.58
MSTRG.2088.1	i	581	LRMDA	10	16.65	0.03	0.44
MSTRG.2089.1	i	520	LRMDA	10	16.45	0.05	0.58

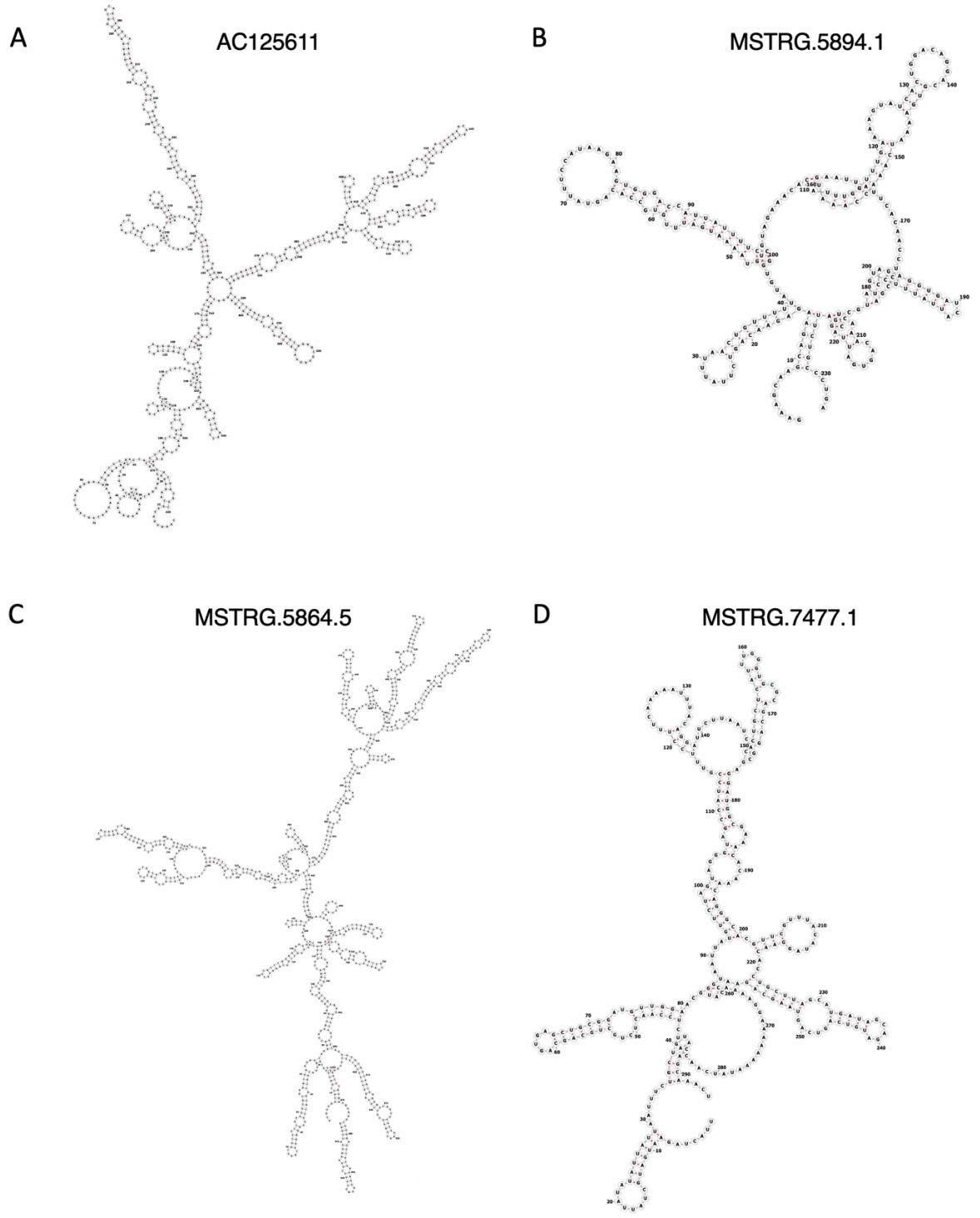

Figure 19. Predicted secondary structures of select *Ripk1*-related lncRNAs. Sequences were obtained from datasets provided by LC Sciences. LncRNAs AC125611(**A**), MSTRG.5894.1 (**B**), MSTRG.5684.5 (**C**), and MSTRG.7477.1 (**D**) were visualized using the RNAfold web server.

4.5 Functional validation of lncRNA candidates

4.5.1 LncRNA expression in inflammation and necroptosis

After designing custom qPCR primers (**Table S3**) for each lncRNA candidate, we analyzed their expression levels in macrophages undergoing inflammation and necroptosis (**Figure 20**). Known lncRNA AC125611, which was upregulated in *Ripk1*-targeted samples that were pulled down following LPS treatment, was also upregulated approximately 2-fold ($p=0.0011$) in cells that were only treated with LPS. AC125611 expression further showed more than a 50% increase ($p=0.0366$) in LPS + zVAD-stimulated cells compared to the NT counterpart.

As for novel lncRNAs MSTRG.5894.1, MSTRG.5684.5, and MSTRG.7477.1, no clear differences in their expression levels were detected across the three conditions. MSTRG.7477.1, which was upregulated in *Ripk1*-targeted samples pulled down after treating with LPS + zVAD, showed around a 30% rise in expression in LPS +/- zVAD-stimulated cells compared to the NT group. However, this change was not statistically significant and thus challenging to conclude.

Regardless of whether we study changes in *Ripk1*-targeted samples with treatments or regular cells with treatments, it is important to note that lncRNA upregulation does not automatically denote its function or activity under a certain condition. These experiments mainly intend to test the ability of our qPCR primers to detect the lncRNAs of interest.

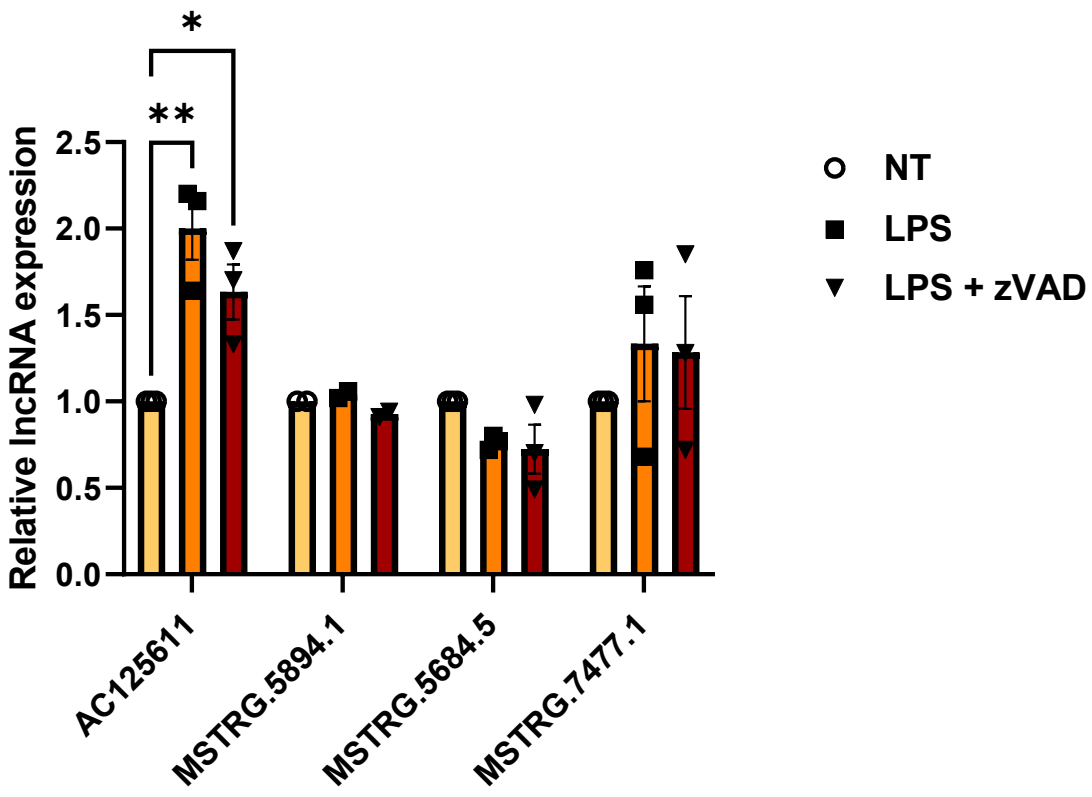

Figure 20. LncRNA expression levels in macrophage inflammation and necroptosis. Cells were treated with 100 ng/ml LPS +/- 50 μM zVAD. After 10 h, RNA was extracted for qPCR analysis of AC125611, MSTRG.5894.1, MSTRG.5684.5, and MSTRG.7477.1. For each lncRNA, results are expressed as fold change relative to the NT control. Data points represent mean ± SEM, n=3 independent experiments. Statistical significance was analyzed by two-way ANOVA and Tukey's multiple comparison test, *$p<0.05$, **$p<0.01$.

4.5.2 Validation of lncRNA knockdowns

Before evaluating the effects of select lncRNAs on *Ripk1* expression, we checked whether transfecting macrophages with locked nucleic acid (LNA) gapmeRs (**Table S4**), custom-designed to target lncRNAs for degradation, led to their successful knockdowns. GapmeR validation was done by comparing lncRNA expression in samples with the corresponding gapmeR to those with a negative control gapmeR. Fold changes < 1 indicating lowered lncRNA expression then prompted us to analyze *Ripk1* expression in these samples.

In NT cells at 6 h post-transfection, lncRNAs AC125611, MSTRG.5894.1, and MSTRG.5684.5 were all significantly knocked down (p=0.0127, 0.0091, and 0.0204, respectively) by over 50% (**Figure 21A**). Compared to the negative control, lncRNA MSTRG.7477.1 expression also decreased by about 30% at 6 h (p=0.3195). Knockdowns for each lncRNA were unexpectedly less potent at 24 h following transfection. Although MSTRG.5684.5 expression was reduced by 40% (p=0.0863), relative levels of the other three lncRNAs were closer to 1.

When macrophages were treated with LPS after transfecting with gapmeRs, 6 h time points did not consistently lead to greater lncRNA knockdowns (**Figure 21C**). At 6 h, AC125611 and MSTRG.7477.1 were around 30% knocked down (p=0.7065 and 0.4555, respectively). MSTRG.7477.1 and MSTRG.5894.1 were also knocked down by roughly 20% or more (p=0.6075 and 0.8140, respectively) at 24 h post-transfection.

Under LPS + zVAD conditions, we further observed slightly lower fold change values at 6 h compared to the 24 h transfection time (**Figure 21E**). While it was unusual to see higher rather than lower MSTRG.5894.1 expression at 24 h, our ability to draw an exact conclusion for this data

is limited by the large variability between replicates. The 6 h time point showed consistent AC125611 and MSTRG.7477.1 knockdowns of approximately 30% (p=0.9686 and p=0.9736, respectively). For both lncRNAs, this extent of decrease resembled that in the LPS treatment at 6 h post-transfection.

Overall, the strongest and most significant lncRNA knockdowns occurred in AC125611, MSTRG.5894.1, and MSTRG.5684.5 after NT macrophages were transfected for 6 h. In contrast, lncRNA knockdowns were the least prominent in LPS + zVAD-treated macrophages at either time point. Of the four lncRNA candidates, MSTRG.7477.1 expression was most consistent in terms of being reduced across the various treatment conditions.

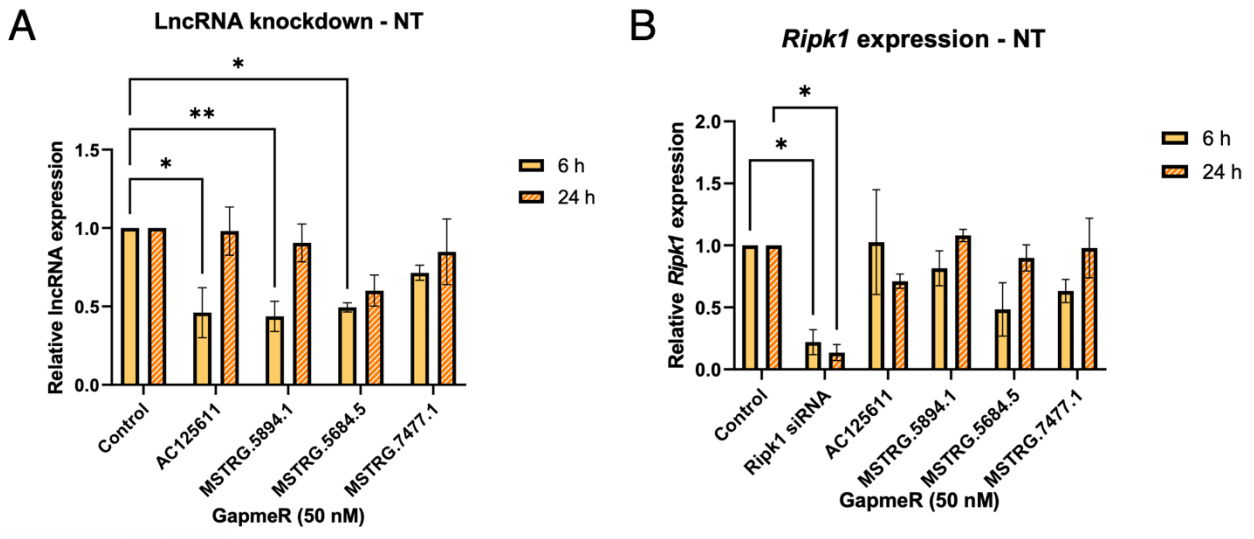

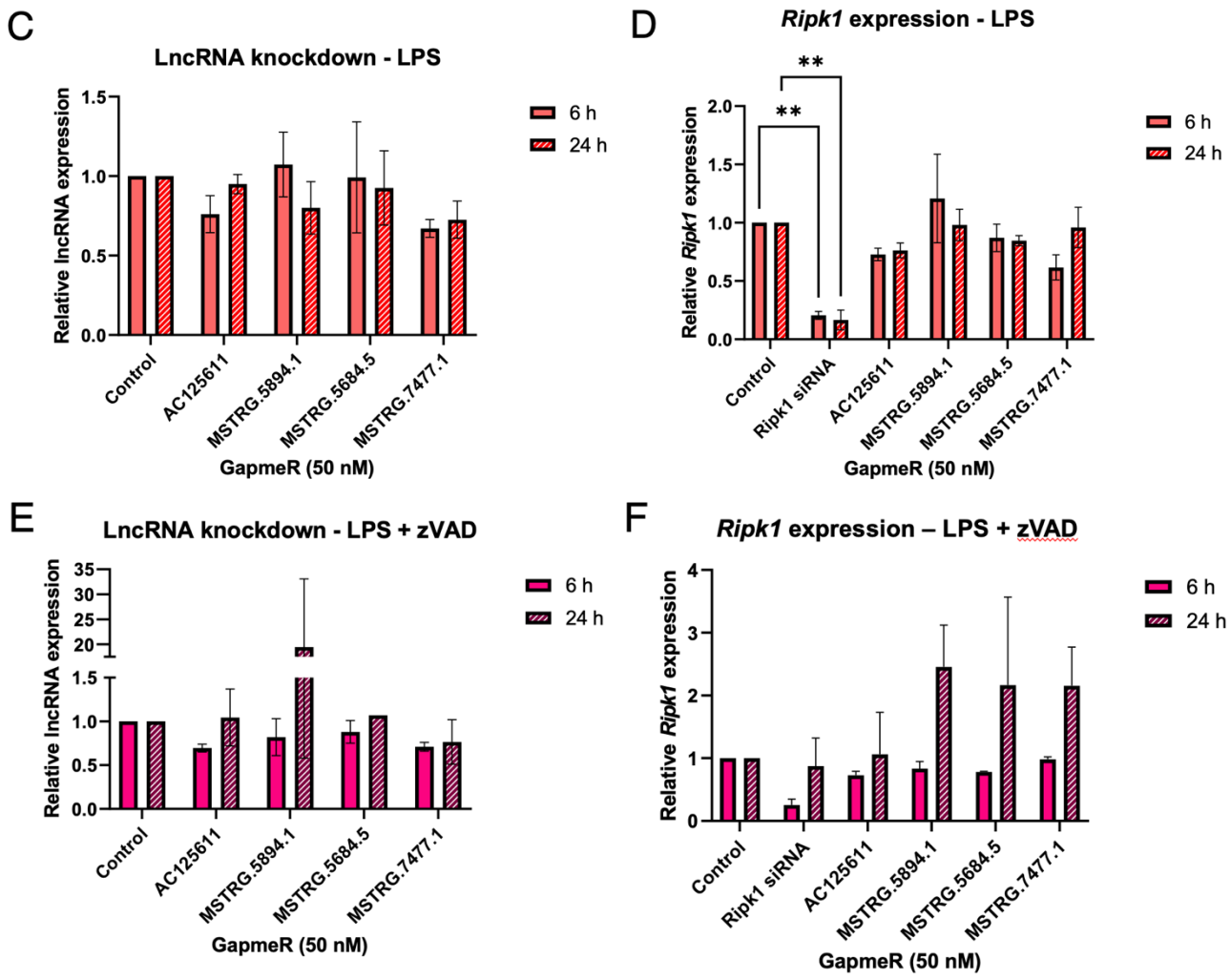

Figure 21. LncRNA and *Ripk1* expression after gapmeR transfections and cell treatments. At 6 h and 24 h post-transfection with 50 nM gapmeRs, macrophages were treated with 100 ng/ml LPS +/- 50 μM zVAD for another 6 h. RNA was then extracted for qPCR analysis of lncRNAs AC125611, MSTRG.5894.1, MSTRG.5684.5, MSTRG.7477.1, and *Ripk1* mRNA under NT (**A-B**), LPS (**C-D**), and LPS + zVAD (**E-F**) treatment conditions. Results are expressed as fold change relative to the negative control. Data points represent mean ± SEM, n=3 independent experiments for NT and LPS conditions, n=2 for LPS + zVAD condition. Statistical significance was analyzed by two-way ANOVA and Dunnett's multiple comparison test, *p<0.05, **p<0.01.

4.5.3 *Ripk1* mRNA expression after lncRNA knockdown

Figure 21 also shows *Ripk1* expression in macrophages transfected with gapmeRs under inflammatory and necroptotic conditions. Significant and potent reductions in *Ripk1* ranging from 78% to 86% were only achieved using the positive control siRNA for the NT and LPS treatment ($p<0.05$ and <0.01, respectively). In samples treated with LPS + zVAD, *Ripk1* knockdown was not significant but still more effective at 6 h post-transfection than at 24 h, given their relative decreases of 74% and 13%.

In the NT condition, significant lncRNA knockdowns of MSTRG.5894.1 and MSTRG.5684.5 at 6 h led to corresponding decreases of 18% and 51% ($p=0.9120$ and 0.1702, respectively) in *Ripk1* expression compared to the negative control (**Figure 21B**). MSTRG.7477.1 knockdown at 6 h also reduced *Ripk1* by 37% ($p=0.4519$). Such findings were unlike the lncRNA knockdown effects on *Ripk1* at 24 h, which were less noticeable.

With LPS treatments, *Ripk1* changes from the control were limited in samples with effective knockdowns (**Figure 21D**). Reduced AC125611 expression led to a 32% decrease in *Ripk1* expression ($p=0.5564$) at 6 h, although a far weaker knockdown of this lncRNA at 24 h similarly resulted in a *Ripk1* decline by 24% ($p=0.6753$). We also remarked that MSTRG.7477.1 knockdown at 6 h post-transfection coincides with a fall in *Ripk1* expression by 38% ($p=0.2520$).

In LPS + zVAD-treated macrophages, weaker lncRNA knockdowns led to less pronounced decreases in *Ripk1* (**Figure 21F**). At 6 h post-transfection, reductions in AC125611, MSTRG.5894.1, and MSTRG.5684.5 ranging from 12% to 30% generally led to reductions in *Ripk1* ranging from 16% to 27%. Meanwhile, *Ripk1* expression barely changed following

MSTRG.7477.1 knockdown at 6 h, and surprisingly increased over 2-fold at 24 h. Similar rises in *Ripk1* expression were also observed in cells with MSTRG.5894.1- and MSTRG.5684.5-targeting gapmeRs, though they did not downregulate the lncRNAs.

From these experiments altogether, we found that lncRNA knockdowns at 6 h were more effective and more frequently led to reduced *Ripk1* expression than those at 24 h post-transfection. Regardless of the treatment administered, we were largely unable to achieve *Ripk1* downregulation in macrophages at this later time point, even after successfully knocking down the related lncRNAs. *Ripk1* downregulation was also more challenging for LPS + zVAD-treated cells, given the weaker lncRNA knockdowns. As for specific lncRNAs standing out from these 6 h analyses, we noted *Ripk1* expression levels paralleled MSTRG.7477.1 knockdowns in normal conditions and inflammation, as well as AC125611 knockdowns in inflammation and necroptosis.

4.5.4 LncRNA expression after *Ripk1* knockdown

To explore the opposite possibility of *Ripk1* affecting the lncRNAs, we examined their levels in macrophages transfected with *Ripk1*-targeting siRNA. **Figure 22** features qPCR data for the four lncRNAs after knocking down *Ripk1* at 6 h and 24 h time points under normal, inflammatory, and necroptotic conditions. Fold changes were calculated by comparing lncRNA expression in these positive control siRNA samples to that of negative control gapmeR samples.

In the NT condition (**Figure 22A**), *Ripk1* knockdowns led to MSTRG.5894.1 and MSTRG.7477.1 expression lowering by approximately 50% and 30% at 6 h post-transfection. Downregulation of the other two lncRNAs AC125611 and MSTRG.5684.5 were either absent or much less pronounced. In contrast, mild to moderate upregulation of these four lncRNAs was interestingly observed at the 24 h mark.

Under LPS- induced inflammation (**Figure 22B**), notable decreases in lncRNA expression were around 25% and mainly seen for MSTRG.5684.5 and MSTRG.7477.1 at 6 h after transfecting cells with *Ripk1*-targeting siRNA. The rest of the data, either at 6 h or 24 h, showed relative lncRNA expression levels hovering around 1 or above. Similarly, with the LPS + zVAD treatment (**Figure 22C**), changes were minimal across the four lncRNAs at both time points.

Taking this data into consideration with the rest, the 6 h time point again proves to be more suitable for observing lncRNA changes. At 6 h post-transfection, silencing *Ripk1* by siRNA leads to obvious reductions in MSTRG.5894.1 for NT cells, MSTRG.5684.5 for LPS-treated cells, and MSTRG.7477.1 in all three. As for the other lncRNAs of interest that are linked to different times and conditions, we can consider their effects on *Ripk1* to be non-reciprocal.

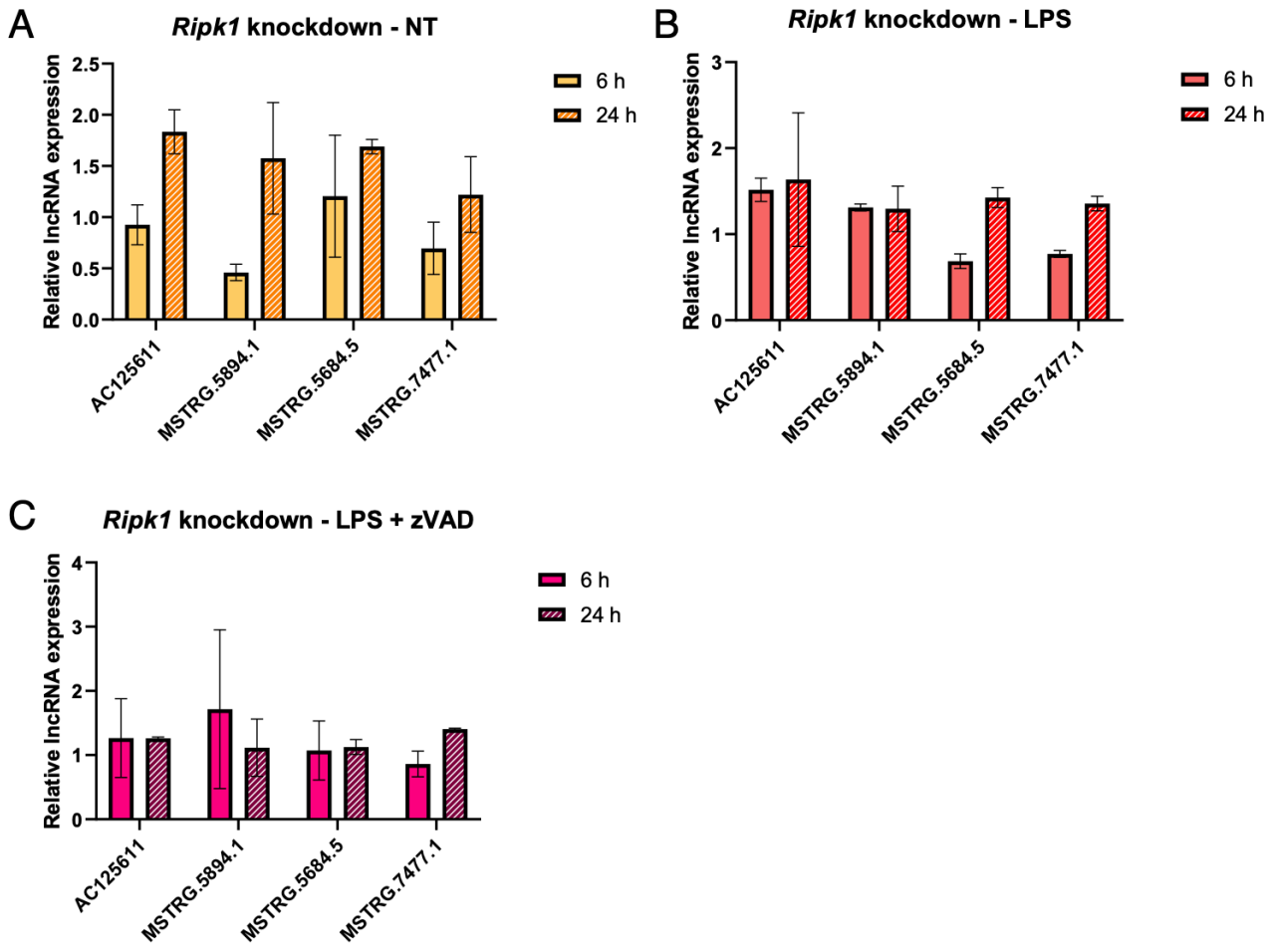

Figure 22. Relative expression of lncRNA candidates after knocking down *Ripk1*. After 6 h and 24 h of transfection with 50 nM *Ripk1*-targeting siRNA, macrophages were treated with 100 ng/ml LPS +/- 50 μM zVAD for 6 h. RNA was then extracted for qPCR analysis of lncRNAs AC125611, MSTRG.5894.1, MSTRG.5684.5, and MSTRG.7477.1 in unstimulated, inflammatory, and necroptotic cells. Results are expressed as fold change relative to the NT control. Data points represent mean ± SEM, n=2 independent experiments.

4.5.5 RIPK1 protein expression after lncRNA knockdown

After reviewing the qPCR results, our lncRNAs of interest were knocked down again in NT and LPS-treated macrophages, given that the effects on *Ripk1* were most pronounced for these conditions. To investigate how RIPK1 changes after cells are transfected with lncRNA-targeting gapmeRs, we collected protein samples at both 6 h and 24 h time points for western blot analysis.

As seen in **Figure 23A-B**, NT macrophages did not display distinct changes in RIPK1 expression between the different gapmeR transfections. At 6 h, the RIPK1 band corresponding to the *Ripk1*-targeting siRNA was visible on the blot but difficult to distinguish from that of the non-targeting gapmeR. In contrast, disappearance of the RIPK1 band at 24 h reveals that RIPK1 silencing was eventually achieved in this positive control.

Figure 23C-D shows RIPK protein levels at 6 h and 24 h following gapmeR transfection and LPS-induced inflammation. RIPK1 knockdown by the positive control siRNA was not established at either time point after treating macrophages with LPS. However, the RIPK1 bands linked to gapmeRs targeting MSTRG.5684.5 and MSTRG.7477.1 were much fainter compared to the negative control at 6 h. RIPK1 differences after knocking down these two lncRNAs were then harder to detect at 24 h. Interestingly, RIPK1 protein expression was more prominent in cells transfected with AC125611- and MSTRG.5894.1-targeting gapmeRs than in those transfected with the non-targeting gapmeR.

Overall, RIPK1 changes at the protein level appear to be more limited than those at the mRNA level. Nonetheless, knocking down MSTRG.5684.5 and MSTRG.7477.1 at the 6 h time point led to less RIPK1 protein expression in LPS-treated macrophages. This finding suggests that

MSTRG.5684.5 and MSTRG.7477.1 may play roles in positively regulating RIPK1. These novel lncRNAs are thus interesting candidates for further study and potential targeting in inflammatory environments where RIPK1 levels are especially elevated.

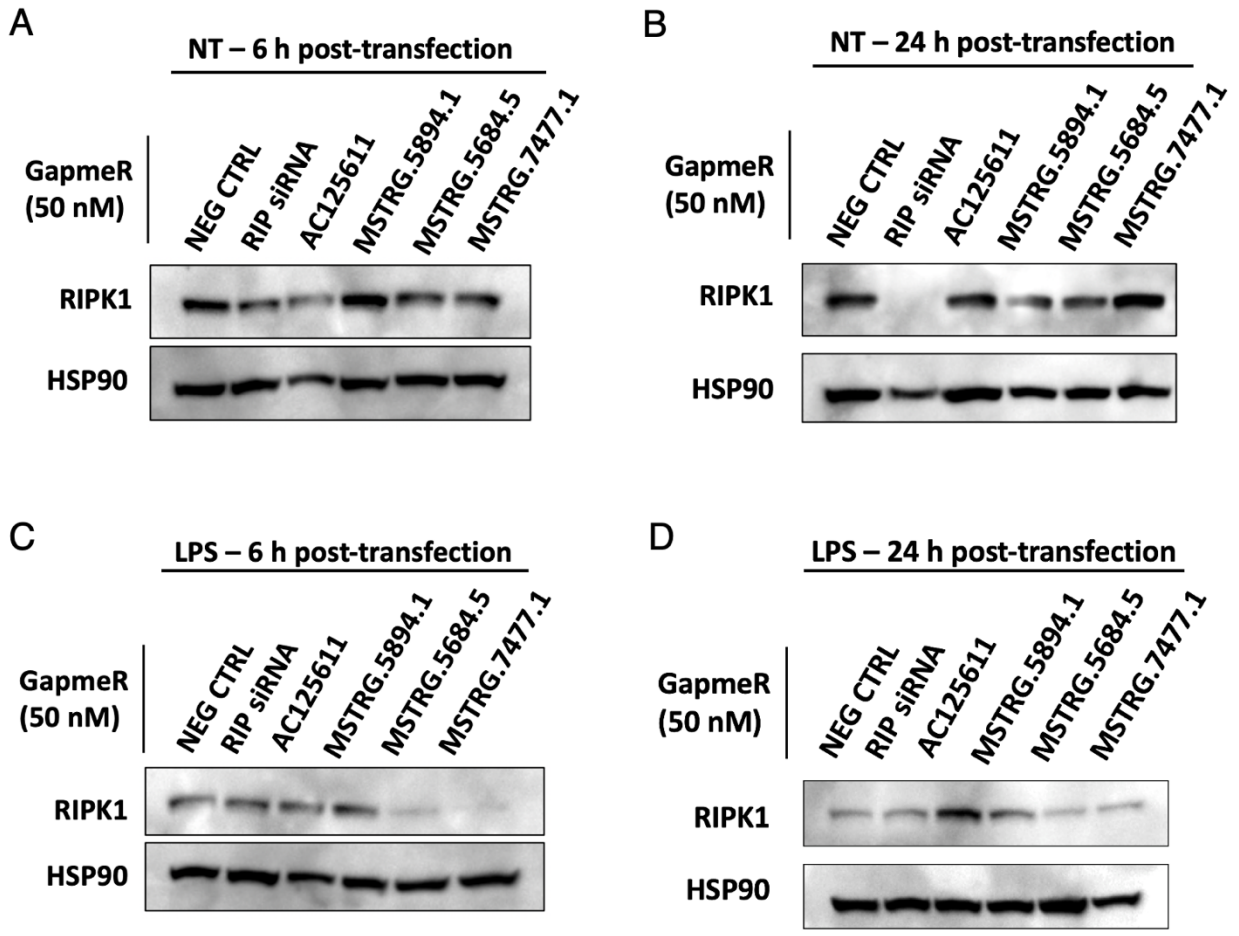

Figure 23. RIPK1 protein levels after transfecting with gapmeRs and inducing inflammation. At 6 h and 24 h post-transfection with 50 nM gapmeRs, macrophages were either left untreated or treated with 100 ng/ml LPS for another 6 h. RNA was then extracted for western blot analysis of RIPK1 under normal (**A-B**) and inflammatory (**C-D**) conditions. HSP90 was used as the protein loading control. Data are representative of n=2 independent experiments.

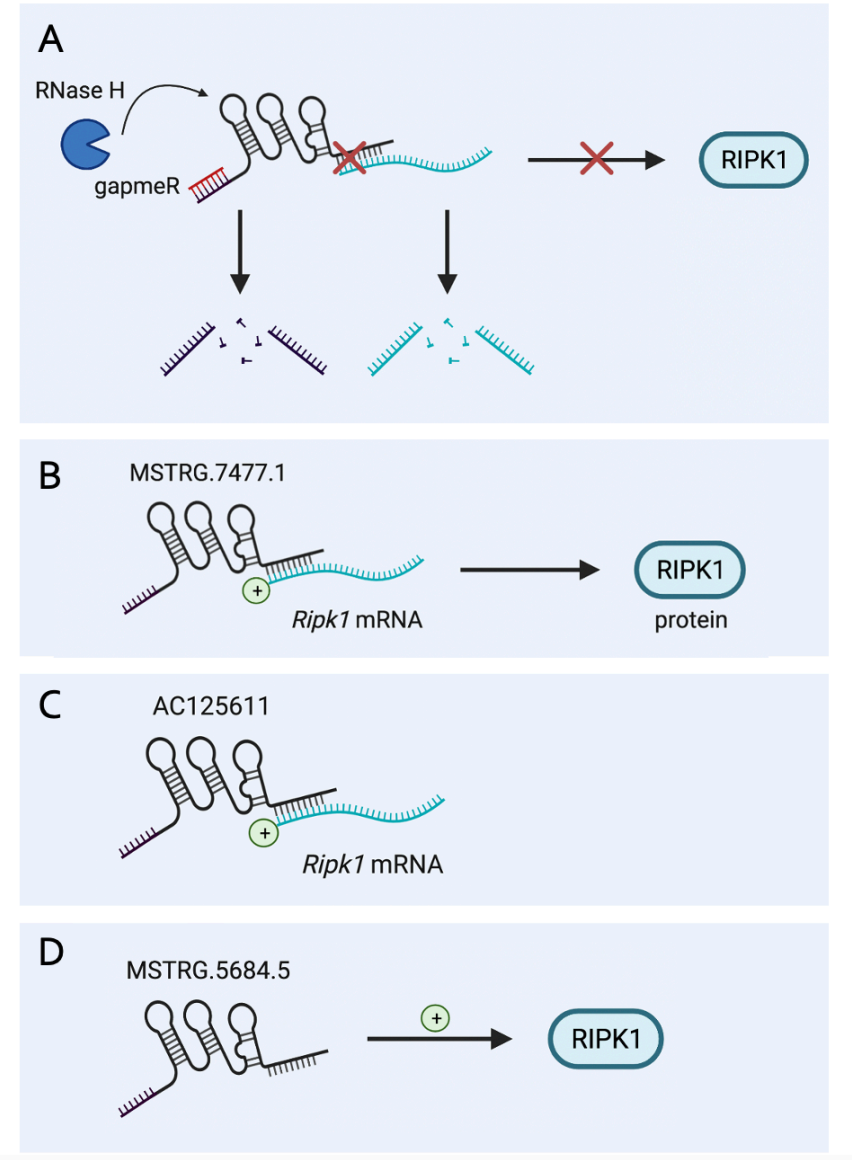

Figure 24. LncRNA knockdowns lead to reductions in *Ripk1* mRNA and/or RIPK1 protein. (**A**) When a specific gapmeR binds MSTRG.7477.1 to recruit RNase H to degrade the lncRNA, MSTRG.7477.1 can no longer positively regulate *Ripk1* mRNA. This may interfere with the stability and/or expression of the mRNA transcript, which in turn causes less RIPK1 protein to be synthesized. (**B**) LncRNA MSTRG.7477.1 may positively regulate *Ripk1* mRNA, which is consequently translated into RIPK1 protein. (**C**) LncRNA AC125611 may positively regulate *Ripk1* mRNA. (**D**) LncRNA MSTRG.5684.5 may positively regulate RIPK1 protein.

5.0 DISCUSSION

Gene expression control comprises a series of regulated changes at multiple levels, from mRNA transcription and translation to protein stability and degradation. In this present study, we examined *Ripk1*-related lncRNA expression profiles in mouse macrophages undergoing inflammation and necroptosis. These processes are largely dependent on the post-translational modifications of RIPK1 and key to inflammatory diseases like atherosclerosis. To identify potentially important lncRNAs associated with *Ripk1* mRNA, we optimized an RNA pull-down assay to generate and analyze transcriptomic data. We also investigated how these lncRNAs may regulate RIPK1 at the mRNA and protein levels by transfecting cells with lncRNA-targeting gapmeRs. Afterwards, we carried out mRNA decay assays and protein degradation assays to determine *Ripk1* mRNA and RIPK1 protein turnover rates, providing further insights into the post-transcriptional control of this major signaling molecule under normal conditions and inflammation.

5.1 Inflammation and necroptosis change *Ripk1* mRNA and related lncRNA levels

The first objective was to study *Ripk1* mRNA expression and *Ripk1*-related lncRNA expression in our conditions of interest. Prior to performing pull-downs, qPCR analysis confirmed the presence of *Ripk1* mRNA and its elevated levels during LPS-induced inflammation and LPS + zVAD-induced cell death. The latter process is known to cause necroptosis, which involves RIPK1 kinase activity and corresponds to the increased release of LDH upon cell membrane disruption. These results are consistent with past studies demonstrating increased *Ripk1* expression in the macrophages of mice with atherosclerosis (24, 25).

Sequencing data and DE analysis later revealed many upregulated lncRNAs in *Ripk1* mRNA-enriched samples under inflammatory and necroptotic conditions. We implemented specific criteria to select key candidates, which include known lncRNA AC125611 and novel lncRNAs MSTRG.5894.1, MSTRG.5684.5, and MSTRG.7477.1. Studies in the literature reporting on AC125611 are limited, but it has been found to be highly expressed in human hepatocellular carcinoma (71) and downregulated in lung adenocarcinoma (72). We further remarked that AC125611 expression was significantly increased in macrophages treated with LPS +/- zVAD. To our knowledge, this is the first evidence of AC125611 involvement in mouse macrophage inflammation and necroptosis.

As our identification and understanding of lncRNA levels rely on outputs from RNA pull-downs, it is necessary to note certain limitations with this method. One limitation concerns the low amounts of *Ripk1* mRNA available for analysis, as revealed by the ddPCR data. This made it difficult to detect significant differences in *Ripk1* expression between targeted and non-targeted BASO groups. Optimization of RNA pull-downs also requires considering the trade-off between sensitivity and specificity. While adding more BASOs that target regions of the *Ripk1* mRNA can increase the chances of capture, non-specific binding and other background noise can likewise increase as an unwanted side effect (73). Distinguishing specific RNA-RNA interactions from non-specific ones is further difficult because these interactions can occur by random collision and pairing, where energy differences are often insignificant (74).

Low amounts of total RNA were another weakness, which was observed when preparing pulled-down RNA samples for next-generation sequencing. Spin column-based purification and DNase treatment further reduced RNA concentrations alongside quality, as seen by the

Bioanalyzer reports. These limitations carry into the sequenced data, since inequivalent RIN assignments reflecting different degrees of degradation can interfere with gene expression quantification and DE analysis (75). To counteract this variability, we generated biological triplicates based on the general requirements for RNA sequencing. In addition, we requested rRNA depletion, which is recommended for low-quality RNA samples and ncRNA studies (76).

5.2 *Ripk1* mRNA and RIPK1 protein stability are influenced by inflammation

mRNA expression is controlled largely by its own turnover within the cell and degradation caused by other molecules. Protein levels depend on their translation and degradation, which in turn depends on the amount of mRNA. Determining that both *Ripk1* mRNA and RIPK1 protein half-lives are approximately 3 h and relatively short is thus relevant to the second study objective, as well as our overall understanding of *Ripk1* gene expression and its regulatory mechanisms in response to surrounding conditions.

We also discovered that treating macrophages with LPS overnight before transcription and translation inhibition respectively increases *Ripk1* mRNA and RIPK1 protein stability. This aligns with our earlier observation regarding *Ripk1* upregulation due to LPS, which activates the TLR4 pathway and eventually pro-inflammatory gene production. More copies of the *Ripk1* transcript or RIPK1 protein may allow for greater resistance to degradation once the transcription or translation machinery is disrupted and new molecules are no longer synthesized.

Enhanced *Ripk1* stability may also stem from various molecular modifications occurring under LPS stimulation. Many factors can influence mRNA turnover, including small RNAs, ARE mutations, and stabilizing or destabilizing RBPs, although their relative contributions remain

unclear (39). Sometimes, protein turnover rates are based on their specific function and cellular location. Those that are actively being used and closer to the cell surface are usually short-lived to enable swift, fine-tuned regulation (77), which is logical when we consider the scaffold function of RIPK1 during inflammation.

On the other hand, co-treating macrophages with LPS and ActD or CHX did not considerably extend *Ripk1* mRNA or RIPK1 protein stability compared to normal conditions without LPS. This signifies the timing and duration of LPS treatment as essential aspects to consider, as its mere presence is not enough. It is also possible that these inhibitors prevent the inflammatory stimulus from promoting pathways and effects that involve RIPK1. The inhibition caused by either ActD or CHX already induces substantial stress, which can eventually stop cellular growth and skew stability measurements (64, 78). The other weakness inherent in protein decay assays is the variability associated with performing Western blots and quantifying band intensities, which can further interfere with accurate RIPK1 half-life determination.

5.3 LncRNA knockdowns in inflammatory macrophages affect *Ripk1* expression

Functional validation of the four lncRNAs selected from RNA sequencing analyses involved introducing custom gapmeRs to blunt their expression, allowing for RIPK1 observations at the mRNA and protein levels. A similar approach has been used to study MALAT1 regulation in macrophage inflammation, where specific gapmeRs were transfected before stimulating with LPS (79). GapmeR knockdowns are the reliable standard for investigating lncRNAs when their subcellular localization in the nucleus or cytoplasm is unknown (80). Our lncRNAs of interest varied in terms of knockdown success and subsequent effects on *Ripk1*, depending on a multitude of factors such as treatment type and time after transfection. However, the lncRNAs that were

effectively knocked down under certain conditions either led to no change in *Ripk1* or less *Ripk1* expression compared to the negative control group.

5.3.1 MSTRG.7477.1 may positively regulate *Ripk1* mRNA and RIPK1 protein

Of the four lncRNA candidates, MSTRG.7477.1 emerges as the most promising because its knockdown in macrophages at 6 h post-transfection consistently correlates to reduced *Ripk1* expression (**Figure 24A**). Although MSTRG.7477.1 was upregulated in RNA samples pulled down by *Ripk1*-targeting BASOs following treatments for necroptosis, these findings from gapmeR experiments were most conspicuous under normal and inflammatory conditions. Furthermore, *Ripk1* silencing by siRNA led to less MSTRG.7477.1 expression, which reflects a reciprocal relationship between this lncRNA and our mRNA of interest. This suggests that MSTRG.7477.1 may be interacting with *Ripk1* mRNA to stabilize or promote its expression in a post-transcriptional manner (**Figure 24B**).

Western blot analysis later revealed less RIPK1 when MSTRG.7477.1 was downregulated at 6 h post-transfection in macrophages subject to LPS-induced inflammation. This discovery is relevant to our previous CHX experiments illustrating that RIPK1 has a short half-life of approximately 3 h. The relative instability of this target protein means less time is expected for it to degrade (81), which may shed light on its susceptibility to downregulation via gapmeR-mediated mRNA degradation. These *Ripk1* changes may be more pronounced at 6 h post-transfection compared to those at 24 h due to the transient effects of the knockdown and additional time for resynthesizing both mRNA and protein.

Not only does this align with previous results showing *Ripk1* and MSTRG.7477.1 co-expression, but it also suggests that the novel lncRNA plays a considerable role in influencing RIPK1 protein. MSTRG.7477.1 is thus an interesting lncRNA for further study and potential targeting in circumstances such as inflammation, where RIPK1 levels are notably high.

5.3.2 AC125611 may positively regulate *Ripk1* mRNA

Knockdown of known lncRNA AC125611 in macrophages at 6 h post-transfection resulted in reduced *Ripk1* expression during inflammation. This effect was similarly seen in cells subject to LPS + zVAD-induced necroptosis but to a lesser extent. As determined through sequencing and DE analysis, AC125611 was originally upregulated in samples stimulated by LPS alone with RNA pulled down by *Ripk1*-targeting BASOs. Knocking down *Ripk1* by siRNA did not cause a corresponding decrease in AC125611, which indicates that the lncRNA is still expressed when *Ripk1* is silenced under both normal and inflammatory conditions. Overall, these findings support the possibility of AC125611 interacting with *Ripk1* mRNA to regulate its expression (**Figure 24C**) under inflammatory conditions.

However, these mRNA changes did not lead to reduced RIPK1 protein in the same situation. This discrepancy may be due to the temporal delay in the correlation between mRNA and protein expression during translation (82). It is also uncertain whether the AC125611-targeting gapmeR caused off-target effects, altering conditions in the cell or accelerating translation of proteins like RIPK1. Another explanation may be that the AC125611 knockdown and corresponding decline in *Ripk1* were not strong enough to prevent existing mRNA copies from being translated into RIPK1 protein. Since mRNA serves as a template for protein production, it

makes sense that proteins are more easily synthesized when an adequate supply of mRNA molecules is available (83).

5.3.3 MSTRG.5684.5 may positively regulate RIPK1 protein

The other novel lncRNA of interest is MSTRG.5684.5. Introducing the corresponding gapmeR to macrophages treated with LPS led to a decline in RIPK1 protein at 6 h and 24 h post-transfection, although this effect was far more pronounced at the earlier time point. Sequencing data showed MSTRG.5684.5 upregulation in samples subject to LPS and *Ripk1*-targeting BASOs. MSTRG.5684.5 also revealed less expression after *Ripk1* silencing by siRNA for 6 h, which provides further evidence of a link between the lncRNA and mRNA. However, MSTRG.5684.5-targeting gapmeR validation was unsuccessful in the LPS condition, as the lncRNA expression did not decrease. This makes it challenging to fully understand how MSTRG.5684.5 may regulate RIPK1 protein levels (**Figure 24D**) through *Ripk1* mRNA.

The main question concerns why MSTRG.5684.5 did not appear to be knocked down in LPS-stimulated macrophages. Because lncRNAs are known to adopt many conformational changes that vary according to specific cellular environments, we speculate that the complex secondary structure of MSTRG.5684.5 may play a role. Although MSTRG.5684.5 expression was lowered by its gapmeR in the NT condition, the same gapmeR may not have effectively accessed its target in the LPS treatment condition, thereby failing to achieve a similar effect.

Such structural variability also makes it plausible that MSTRG.5684.5 was indeed knocked down, but there were challenges with qPCR primers binding the lncRNA consistently to detect its expression. It is also possible for changes in lncRNA expression to be reflected in the target protein

but not at the mRNA level, as seen in a similar study (84). In this case, MSTRG.5684.5 may take part in regulating RIPK1 protein translation rather than *Ripk1* mRNA expression or stability. However, these current interpretations still limit us from drawing a firm conclusion about MSTRG.5684.5, so further investigations are needed.

5.4 Future directions and implications for studying *Ripk1*-related lncRNAs

There are many paths to advancing our knowledge of these lncRNAs and their effects on RIPK1-mediated inflammation and necroptosis. One priority is to improve the lncRNA knockdown experiments and to understand why transfection outcomes vary depending on cell treatments and time points. The gapmeRs seem to be less effective at knocking down target lncRNAs to cause corresponding *Ripk1* reductions in necroptotic environments, but the reasons for this remain unclear. Optimization may require adding multiple gapmeRs to enhance target specificity and adjusting their concentrations to increase knockdown efficiency, while minimizing potential toxic or off-target effects (80). Another question surrounds the size of our knockdowns and whether the lack of statistical significance still generates useful effects in macrophages. Repeating these experiments to collect and analyze more replicates can help to confirm these uncertainties.

As for additional lncRNA studies, it may be worthwhile to overexpress lncRNAs of interest with viral-mediated gene delivery to observe whether *Ripk1* and RIPK1 expression concurrently changes. Pro-inflammatory cytokine upregulation, increased cell death, and other pertinent effects should also be assessed to understand how lncRNA manipulation alters RIPK1-mediated inflammatory and necroptotic pathways. For promising candidates like MSTRG.7477.1, we may combine gapmeR transfections with CHX chase assays to investigate lncRNA knockdown effects

on RIPK1 protein stability during macrophage inflammation. It is also important to elucidate their location in macrophages, their specific mechanism for regulating *Ripk1*, and their conservation between mice and humans. Pinpointing the subcellular localization of a lncRNA can hint at its function. LncRNAs in the nucleus often act as scaffolds to regulate mRNA processing, while those in the cytoplasm can influence mRNA translation to protein (85). This is critical to developing optimal methods for lncRNA targeting and evaluating their feasibility for clinical applications.

Other limitations of this project represent opportunities for further exploration. Our pull-downs focused on analyzing lncRNAs physically attached to *Ripk1* mRNA, but it is likely that lncRNA-mRNA interactions belong to larger networks and involve other molecules. In the future, we may use RNA immunoprecipitation assays to examine interactions between *Ripk1* mRNA and various proteins, some of which may be RBPs recruited by associating lncRNAs (86). As we solely relied on the RAW 264.7 murine macrophage cell line for experimentation here, we may consider testing *Ripk1*-related lncRNAs in primary cells like BMDMs next. The two cell types have been reported to resemble each other in phenotype and in response to TLR4 activation by ligands like LPS (87). However, it is still beneficial to verify the presence of relevant lncRNAs in different macrophages and whether they affect *Ripk1* as expected. Functional gapmeRs that effectively target lncRNAs found to control RIPK1 levels could eventually be applied to mouse models for inflammatory disease.

Our study sets the ground for future preclinical and clinical developments to counteract the high levels of RIPK1 characteristic of macrophage inflammation, which is common to many pathological processes including atherosclerosis. Knocking down key lncRNAs to downregulate *Ripk1* at the post-transcriptional level could be an attractive therapeutic approach, particularly

when there is high targetability and specificity. Targeting *Ripk1*-regulating lncRNAs that are specifically expressed in inflammation may even be more effective than directly blocking RIPK1, which can simultaneously take part in multiple pathways for cell survival and cell death (4). Once developed and validated, lncRNA inhibitors could be used in combination with standard therapies to reduce RIPK1-mediated inflammation in atherosclerosis and other diseases.

5.5 Conclusions

To our knowledge, this is the first study to report on the post-transcriptional mechanisms surrounding RIPK1 at the mRNA and protein levels in macrophage inflammation. LncRNAs interacting with the *Ripk1* transcript, along with the turnover of mRNA and protein, all contribute to the post-transcriptional control of RIPK1. Here, we have identified key *Ripk1*-related lncRNAs from RNA pull-downs followed by sequencing. Knocking down lncRNAs and inducing inflammation in cells showed that AC125611 influences *Ripk1* mRNA expression, MSTRG.5894.1 influences RIPK1 protein expression, while novel lncRNA MSTRG.7477.1 is most consistent in influencing both. We have also discovered that *Ripk1* mRNA and RIPK1 protein have short half-lives under both normal and inflammatory conditions. This information is helpful for eventually determining an effective strategy to target lncRNAs. Additional studies are surely needed to gain a more comprehensive understanding of their biology before proceeding with clinical translation. Nonetheless, there lies great potential for lncRNA inhibition to alleviate RIPK1 upregulation in atherosclerosis and other diseases where inflammation is prominent.

SUPPLEMENTARY TABLES

Table S1. Antisense oligonucleotide probes targeting various regions of *Ripk1* mRNA.

Location	Start	End	Length	ASO sequence (5'→ 3')
Exons 3-4	450	471	22	AGTGGGACATCTATCTGGGTCT
Exons 5-6	818	839	22	TACAGATGACATTCTCATAGGG
Exons 8-9	1133	1156	24	TCCAGGTTGTTCTGAATTTGACCT
Exons 10-11	1810	1831	22	AGTGGTGTTATCAAAGATGGCT
3' UTR A	3372	3392	21	ACGTTACAGGAGAGTCCCTCC
3' UTR B	4884	4906	23	TAGACATAAATAAATAGATCTAA

Table S2. qPCR primer sequences spanning ASO-binding sites on *Ripk1* mRNA.

Pair	Primer	Sequence (5'→ 3')	Range	Length (bp)	Tm (°C)	GC (%)
1	Fwd	CTGATGCACGTGCTAAAGACCCAG	434–547	24	59.7	54.2
	Rev	GCCTCCACGATTATCCTTCCTTTC	478–501	24	58.2	50.0
2	Fwd	GCTTTGGCATTGTCCTTTGGGCA	777–799	23	63.7	52.2
	Rev	CCAGATTTTATGCAGATCACGAACT	846–870	25	55.6	40.0
3	Fwd	ATCAGCCTCATGGAGCGGTGCT	920–941	22	61.7	59.1
	Rev	GCCTAAATTCTTCTTCAATGCCAAG	974–998	25	56.7	40.0
4	Fwd	TTCACTGCAGCATGACTGTGTACCC	1096–1120	25	59.9	52.0
	Rev	GGAACTGTGCAGCGATCCAG	1152–1171	20	55.5	60.0
5	Fwd	CGACTTCCAGACACCAAGCCATC	1794–1816	23	59.5	56.5
	Rev	GGGTTCAGGTGTTCATCAGTCAGAC	1833–1857	25	57.6	52.0
6	Fwd	TGCTACATGTTCTTTGGAGGGACTC	3357–3381	25	57.5	48.0
	Rev	CTGAGAAACCTTGTCTGGGGATGGG	3400–3424	25	62.6	56.0
7	Fwd	AAAGGAGCCCTGCCTCAAAGACTT	4854–4877	24	59.7	50.0
	Rev	CACAACCATCTGGTCAGCTACAGTG	4913–4937	25	57.5	52.0

Table S3. qPCR primer sequences spanning gapmeR-binding sites on select lncRNAs.

LncRNA	Primer	Sequence (5'→ 3')
AC125611	Fwd	CTG CTC CAA CCT CCT CAT AAT C
	Rev	AGC GTG CCT TTG TTC ACT
MSTRG.5894.1	Fwd	TGT GCC ACA GTA TTT CCA TAA GA
	Rev	TCA CGT CCT GTC CAG TGA TA
MSTRG.5684.5	Fwd	CAG AGT ATG GGA CCT GAA AGA TG
	Rev	CCG ACT GAA CAC AGC ATA GAA
MSTRG.7477.1	Fwd	GGT AGC CAT CCG TTT CCT TT
	Rev	GCT AAG CAG GTG TTC CTA TGT

Table S4. Antisense LNA gapmeRs targeting key lncRNAs for functional validation.

GapmeR target	Sequence (5'→ 3')
AC125611	ATA GTG CTG ACG GAG A
MSTRG.5894.1	AGA ATC CTA ATC ACT G
MSTRG.5684.5	GCG GAC CCA ACA ACA G
MSTRG.7477.1	GCG TGA TTA AGA ATC C

REFERENCES

1. Silke J, Rickard JA, Gerlic M. The diverse role of RIP kinases in necroptosis and inflammation. Nature Immunology. 2015;16(7):689-97.

2. Ofengeim D, Yuan J. Regulation of RIP1 kinase signalling at the crossroads of inflammation and cell death. Nat Rev Mol Cell Biol. 2013;14(11):727-36.

3. Mifflin L, Ofengeim D, Yuan J. Receptor-interacting protein kinase 1 (RIPK1) as a therapeutic target. Nature Reviews Drug Discovery. 2020;19(8):553-71.

4. Wang Q, Fan D, Xia Y, Ye Q, Xi X, Zhang G, et al. The latest information on the RIPK1 post-translational modifications and functions. Biomedicine & Pharmacotherapy. 2021;142:112082.

5. Degterev A, Ofengeim D, Yuan J. Targeting RIPK1 for the treatment of human diseases. Proceedings of the National Academy of Sciences. 2019;116(20):9714-22.

6. Ting AT, Bertrand MJM. More to Life than NF-κB in TNFR1 Signaling. Trends in Immunology. 2016;37(8):535-45.

7. Delanghe T, Dondelinger Y, Bertrand MJM. RIPK1 Kinase-Dependent Death: A Symphony of Phosphorylation Events. Trends in Cell Biology. 2020;30(3):189-200.

8. Annibaldi A, Wicky John S, Vanden Berghe T, Swatek KN, Ruan J, Liccardi G, et al. Ubiquitin-Mediated Regulation of RIPK1 Kinase Activity Independent of IKK and MK2. Mol Cell. 2018;69(4):566-80.e5.

9. Vanlangenakker N, Vanden Berghe T, Vandenabeele P. Many stimuli pull the necrotic trigger, an overview. Cell Death & Differentiation. 2012;19(1):75-86.

10. Najjar M, Saleh D, Zelic M, Nogusa S, Shah S, Tai A, et al. RIPK1 and RIPK3 Kinases Promote Cell-Death-Independent Inflammation by Toll-like Receptor 4. Immunity. 2016;45(1):46-59.

11. Liu Z, Chan FK-M. Regulatory mechanisms of RIPK1 in cell death and inflammation. Seminars in Cell & Developmental Biology. 2021;109:70-5.

12. Filipčík P, Curry JR, Mace PD. When Worlds Collide—Mechanisms at the Interface between Phosphorylation and Ubiquitination. Journal of Molecular Biology. 2017;429(8):1097-113.

13. Polykratis A, Hermance N, Zelic M, Roderick J, Kim C, Van T-M, et al. Cutting Edge: RIPK1 Kinase Inactive Mice Are Viable and Protected from TNF-Induced Necroptosis In Vivo. The Journal of Immunology. 2014;193(4):1539.

14. Shan B, Pan H, Najafov A, Yuan J. Necroptosis in development and diseases. Genes Dev. 2018;32(5-6):327-40.

15. Newton K. RIPK1 and RIPK3: critical regulators of inflammation and cell death. Trends in Cell Biology. 2015;25(6):347-53.

16. Pasparakis M, Vandenabeele P. Necroptosis and its role in inflammation. Nature. 2015;517(7534):311-20.

17. Gupta K, Phan N, Wang Q, Liu B. Necroptosis in cardiovascular disease - a new therapeutic target. Journal of Molecular and Cellular Cardiology. 2018;118:26-35.

18. Kroemer G, Galluzzi L, Vandenabeele P, Abrams J, Alnemri ES, Baehrecke EH, et al. Classification of cell death: recommendations of the Nomenclature Committee on Cell Death 2009. Cell Death & Differentiation. 2009;16(1):3-11.

19. Vanden Berghe T, Kaiser WJ, Bertrand MJM, Vandenabeele P. Molecular crosstalk between apoptosis, necroptosis, and survival signaling. Molecular & Cellular Oncology. 2015;2(4):e975093.

20. Christofferson DE, Yuan J. Necroptosis as an alternative form of programmed cell death. Curr Opin Cell Biol. 2010;22(2):263-8.

21. Degterev A, Hitomi J, Germscheid M, Ch'en IL, Korkina O, Teng X, et al. Identification of RIP1 kinase as a specific cellular target of necrostatins. Nat Chem Biol. 2008;4(5):313-21.

22. Robinson N, Ganesan R, Hegedűs C, Kovács K, Kufer TA, Virág L. Programmed necrotic cell death of macrophages: Focus on pyroptosis, necroptosis, and parthanatos. Redox Biology. 2019;26:101239.

23. Zheng Y, Gardner SE, Clarke MCH. Cell Death, Damage-Associated Molecular Patterns, and Sterile Inflammation in Cardiovascular Disease. Arteriosclerosis, Thrombosis, and Vascular Biology. 2011;31(12):2781-6.

24. Karunakaran D, Geoffrion M, Wei L, Gan W, Richards L, Shangari P, et al. Targeting macrophage necroptosis for therapeutic and diagnostic interventions in atherosclerosis. Science Advances. 2016;2(7):e1600224.

25. Karunakaran D, Nguyen M-A, Geoffrion M, Vreeken D, Lister Z, Cheng HS, et al. RIPK1 Expression Associates With Inflammation in Early Atherosclerosis in Humans and Can Be Therapeutically Silenced to Reduce NF-κB Activation and Atherogenesis in Mice. Circulation. 2021;143(2):163-77.

26. Ofengeim D, Mazzitelli S, Ito Y, DeWitt JP, Mifflin L, Zou C, et al. RIPK1 mediates a disease-associated microglial response in Alzheimer's disease. Proc Natl Acad Sci U S A. 2017;114(41):E8788-E97.

27. Mata J, Marguerat S, Bähler J. Post-transcriptional control of gene expression: a genome-wide perspective. Trends Biochem Sci. 2005;30(9):506-14.

28. Buccitelli C, Selbach M. mRNAs, proteins and the emerging principles of gene expression control. Nature Reviews Genetics. 2020;21(10):630-44.

29. Mercer TR, Dinger ME, Mattick JS. Long non-coding RNAs: insights into functions. Nat Rev Genet. 2009;10(3):155-9.

30. Schoenberg DR, Maquat LE. Regulation of cytoplasmic mRNA decay. Nature Reviews Genetics. 2012;13(4):246-59.

31. Schwanhäusser B, Busse D, Li N, Dittmar G, Schuchhardt J, Wolf J, et al. Global quantification of mammalian gene expression control. Nature. 2011;473(7347):337-42.

32. Hinkson IV, Elias JE. The dynamic state of protein turnover: It's about time. Trends Cell Biol. 2011;21(5):293-303.

33. Cheadle C, Fan J, Cho-Chung YS, Werner T, Ray J, Do L, et al. Control of gene expression during T cell activation: alternate regulation of mRNA transcription and mRNA stability. BMC Genomics. 2005;6(1):75.

34. Garneau NL, Wilusz J, Wilusz CJ. The highways and byways of mRNA decay. Nat Rev Mol Cell Biol. 2007;8(2):113-26.

35. Sheth U, Parker R. Decapping and decay of messenger RNA occur in cytoplasmic processing bodies. Science. 2003;300(5620):805-8.

36. Eulalio A, Behm-Ansmant I, Schweizer D, Izaurralde E. P-body formation is a consequence, not the cause, of RNA-mediated gene silencing. Mol Cell Biol. 2007;27(11):3970-81.

37. Sebastian-delaCruz M, Gonzalez-Moro I, Olazagoitia-Garmendia A, Castellanos-Rubio A, Santin I. The Role of lncRNAs in Gene Expression Regulation through mRNA Stabilization. Non-Coding RNA. 2021;7(1):3.

38. Gong C, Maquat LE. lncRNAs transactivate STAU1-mediated mRNA decay by duplexing with 3′ UTRs via Alu elements. Nature. 2011;470(7333):284-8.

39. Larsson E, Sander C, Marks D. mRNA turnover rate limits siRNA and microRNA efficacy. Mol Syst Biol. 2010;6:433-.

40. Lecker SH, Goldberg AL, Mitch WE. Protein Degradation by the Ubiquitin–Proteasome Pathway in Normal and Disease States. Journal of the American Society of Nephrology. 2006;17(7):1807-19.

41. Maier T, Güell M, Serrano L. Correlation of mRNA and protein in complex biological samples. FEBS Letters. 2009;583(24):3966-73.

42. Zhou P. Determining protein half-lives. Signal Transduction Protocols: Springer; 2004. p. 67-77.

43. Varshavsky A. The N-end rule pathway and regulation by proteolysis. Protein Sci. 2011;20(8):1298-345.

44. Piatkov KI, Brower CS, Varshavsky A. The N-end rule pathway counteracts cell death by destroying proapoptotic protein fragments. Proceedings of the National Academy of Sciences. 2012;109(27):E1839-E47.

45. Hochstrasser M. UBIQUITIN-DEPENDENT PROTEIN DEGRADATION. Annual Review of Genetics. 1996;30(1):405-39.

46. Tani H, Mizutani R, Salam KA, Tano K, Ijiri K, Wakamatsu A, et al. Genome-wide determination of RNA stability reveals hundreds of short-lived noncoding transcripts in mammals. Genome research. 2012;22(5):947-56.

47. Kazimierczyk M, Kasprowicz MK, Kasprzyk ME, Wrzesinski J. Human Long Noncoding RNA Interactome: Detection, Characterization and Function. International Journal of Molecular Sciences. 2020;21(3):1027.

48. Delás MJ, Hannon GJ. lncRNAs in development and disease: from functions to mechanisms. Open Biology. 2017;7(7):170121.

49. Yoon J-H, Abdelmohsen K, Gorospe M. Posttranscriptional Gene Regulation by Long Noncoding RNA. Journal of Molecular Biology. 2013;425(19):3723-30.

50. Bridges MC, Daulagala AC, Kourtidis A. LNCcation: lncRNA localization and function. Journal of Cell Biology. 2021;220(2).

51. Fatica A, Bozzoni I. Long non-coding RNAs: new players in cell differentiation and development. Nature Reviews Genetics. 2014;15(1):7-21.

52. Statello L, Guo C-J, Chen L-L, Huarte M. Gene regulation by long non-coding RNAs and its biological functions. Nature Reviews Molecular Cell Biology. 2021;22(2):96-118.

53. Romero-Barrios N, Legascue MF, Benhamed M, Ariel F, Crespi M. Splicing regulation by long noncoding RNAs. Nucleic Acids Res. 2018;46(5):2169-84.

54. Gong C, Maquat LE. lncRNAs transactivate STAU1-mediated mRNA decay by duplexing with 3' UTRs via Alu elements. Nature. 2011;470(7333):284-8.

55. Carrieri C, Cimatti L, Biagioli M, Beugnet A, Zucchelli S, Fedele S, et al. Long non-coding antisense RNA controls Uchl1 translation through an embedded SINEB2 repeat. Nature. 2012;491(7424):454-7.

56. Huang H, Weng H, Sun W, Qin X, Shi H, Wu H, et al. Recognition of RNA N(6)-methyladenosine by IGF2BP proteins enhances mRNA stability and translation. Nat Cell Biol. 2018;20(3):285-95.

57. Wang K, Liu F, Liu CY, An T, Zhang J, Zhou LY, et al. The long noncoding RNA NRF regulates programmed necrosis and myocardial injury during ischemia and reperfusion by targeting miR-873. Cell Death Differ. 2016;23(8):1394-405.

58. Ma L, Bajic VB, Zhang Z. On the classification of long non-coding RNAs. RNA Biol. 2013;10(6):925-33.

59. Li R, Zhu H, Luo Y. Understanding the Functions of Long Non-Coding RNAs through Their Higher-Order Structures. International journal of molecular sciences. 2016;17(5):702.

60. Tsagakis I, Douka K, Birds I, Aspden JL. Long non-coding RNAs in development and disease: conservation to mechanisms. J Pathol. 2020;250(5):480-95.

61. Gudenas BL, Wang L. Prediction of LncRNA Subcellular Localization with Deep Learning from Sequence Features. Scientific Reports. 2018;8(1):16385.

62. Fok ET, Scholefield J, Fanucchi S, Mhlanga MM. The emerging molecular biology toolbox for the study of long noncoding RNA biology. Epigenomics. 2017;9(10):1317-27.

63. Mathy NW, Chen X-M. Long non-coding RNAs (lncRNAs) and their transcriptional control of inflammatory responses. Journal of Biological Chemistry. 2017;292(30):12375-82.

64. Lai WS, Arvola RM, Goldstrohm AC, Blackshear PJ. Inhibiting transcription in cultured metazoan cells with actinomycin D to monitor mRNA turnover. Methods. 2019;155:77-87.

65. Najjar M, Saleh D, Zelic M, Nogusa S, Shah S, Tai A, et al. RIPK1 and RIPK3 Kinases Promote Cell-Death-Independent Inflammation by Toll-like Receptor 4. Immunity. 2016;45(1):46-59.

66. Taylor S, Wakem M, Dijkman G, Alsarraj M, Nguyen M. A practical approach to RT-qPCR—Publishing data that conform to the MIQE guidelines. Methods. 2010;50(4):S1-S5.

67. Sharova LV, Sharov AA, Nedorezov T, Piao Y, Shaik N, Ko MSH. Database for mRNA Half-Life of 19 977 Genes Obtained by DNA Microarray Analysis of Pluripotent and Differentiating Mouse Embryonic Stem Cells. DNA Research. 2008;16(1):45-58.

68. Toyama BH, Hetzer MW. Protein homeostasis: live long, won't prosper. Nat Rev Mol Cell Biol. 2013;14(1):55-61.

69. Tavares L, Alves PM, Ferreira RB, Santos CN. Comparison of different methods for DNA-free RNA isolation from SK-N-MC neuroblastoma. BMC Research Notes. 2011;4(1):3.

70. Conesa A, Madrigal P, Tarazona S, Gomez-Cabrero D, Cervera A, McPherson A, et al. A survey of best practices for RNA-seq data analysis. Genome Biology. 2016;17(1):13.

71. He Y, Shi Q, Zhang Y, Yuan X, Yu Z. Transcriptome-Wide 5-Methylcytosine Functional Profiling of Long Non-Coding RNA in Hepatocellular Carcinoma. Cancer Manag Res. 2020;12:6877-85.

72. Wang K, Yan T, Liu W, Zhong W, Zhao Q, Du J. A Novel Target PCPB1-AS1 Regulates the Treg Infiltration and Serves as a Potential Biomarker for Immunotherapy Response in Lung Adenocarcinoma. Available at SSRN 3786688.

73. Simon MD, Machyna M. Principles and practices of hybridization capture experiments to study long noncoding RNAs that act on chromatin. Cold Spring Harbor Perspectives in Biology. 2019;11(11):a032276.

74. Gong J, Ju Y, Shao D, Zhang QC. Advances and challenges towards the study of RNA-RNA interactions in a transcriptome-wide scale. Quantitative Biology. 2018;6(3):239-52.

75. Gallego Romero I, Pai AA, Tung J, Gilad Y. RNA-seq: impact of RNA degradation on transcript quantification. BMC biology. 2014;12(1):1-13.

76. Schuierer S, Carbone W, Knehr J, Petitjean V, Fernandez A, Sultan M, et al. A comprehensive assessment of RNA-seq protocols for degraded and low-quantity samples. BMC genomics. 2017;18(1):1-13.

77. Dörrbaum AR, Kochen L, Langer JD, Schuman EM. Local and global influences on protein turnover in neurons and glia. Elife. 2018;7.

78. Alber AB, Suter DM. Dynamics of protein synthesis and degradation through the cell cycle. Cell Cycle. 2019;18(8):784-94.

79. Cui H, Banerjee S, Guo S, Xie N, Ge J, Jiang D, et al. Long noncoding RNA Malat1 regulates differential activation of macrophages and response to lung injury. JCI Insight. 2019;4(4).

80. Yokota T, Maruyama R. Gapmers.

81. Bartlett DW, Davis ME. Insights into the kinetics of siRNA-mediated gene silencing from live-cell and live-animal bioluminescent imaging. Nucleic Acids Res. 2006;34(1):322-33.

82. Becker K, Bluhm A, Casas-Vila N, Dinges N, Dejung M, Sayols S, et al. Quantifying post-transcriptional regulation in the development of Drosophila melanogaster. Nature Communications. 2018;9(1):4970.

83. Gedeon T, Bokes P. Delayed Protein Synthesis Reduces the Correlation between mRNA and Protein Fluctuations. Biophysical Journal. 2012;103(3):377-85.

84. Hu G, Lou Z, Gupta M. The long non-coding RNA GAS5 cooperates with the eukaryotic translation initiation factor 4E to regulate c-Myc translation. PloS one. 2014;9(9):e107016.

85. He J, Tu C, Liu Y. Role of lncRNAs in aging and age-related diseases. Aging Medicine. 2018;1(2):158-75.

86. Bierhoff H. Analysis of lncRNA-protein interactions by RNA-protein pull-down assays and RNA immunoprecipitation (RIP). Cellular Quiescence: Springer; 2018. p. 241-50.

87. Berghaus LJ, Moore JN, Hurley DJ, Vandenplas ML, Fortes BP, Wolfert MA, et al. Innate immune responses of primary murine macrophage-lineage cells and RAW 264.7 cells to ligands of Toll-like receptors 2, 3, and 4. Comp Immunol Microbiol Infect Dis. 2010;33(5):443-54.